Bedrock geology controls on new water fractions and catchment functioning in contrasted nested catchments

Guilhem Türk[1,2*], Christoph J. Gey [3], Bernd R. Schöne [3], Marius G. Floriancic [4,5], James W. Kirchner [5,6,7], Loic Leonard [1], Laurent Gourdol [1], Richard F. Keim [1], Laurent Pfister [1,2]

[1]CATchment and ecohydrology research group, Environmental sensing and modelling unit, Luxembourg Institute of Science and Technology, Belvaux, Luxembourg
[2]Faculty of Science, Technology and Medicine, University of Luxembourg, Belval, Luxembourg
[3]Institute of Geosciences, University of Mainz, Mainz, Germany
[4]Dept. of Civil, Environmental and Geomatic Engineering ETH Zürich, Zürich, Switzerland
[5]Dept. of Environmental Systems Science, 5 ETH Zürich, Zürich, Switzerland
[6]Swiss Federal Research Institute WSL, Birmensdorf, Switzerland
[7]Dept. of Earth and Planetary Science, University of California, Berkeley, CA, USA

Correspondence to: Guilhem Türk (guilhem.turk@hotmail.com) or Laurent Pfister (laurent.pfister@list.lu)

Abstract. We still lack substantial understanding on how landscape characteristics shape the storage and release of water at the catchment scale. Here we use 13 years of fortnightly precipitation and streamflow $\delta^{18}O$ measurements together with hydrometeorological data from 12 nested catchments (0.5 to 247.5 km^2) in the Alzette River basin (Luxembourg) to study bedrock geology and landcover controls on streamflow generation.

Streamflow responses to precipitation were highly variable. Runoff coefficients were typically higher in catchments dominated by less permeable bedrock (i.e. marls and claystones, R_c = 0.43 to 0.52) than in catchments with a high fraction of permeable bedrock (i.e. sandstones and conglomerates, R_c = 0.19 to 0.40). The fraction of new water (F_{new}, water younger than ~ 16 days in this study) determined via ensemble hydrograph separation was strongly related to differences in bedrock geology. F_{new} was highest in impermeable bedrock catchments (i.e. with a dominance of marls and claystone, F_{new} = 4.5 to 11.9%), increasing with higher specific daily streamflow (F_{new} up to 45% in one catchment). In catchments with an important fraction of permeable sandstone and conglomerates, high F_{new} variability with specific streamflow (F_{new} rising to 25% in one catchment) was also found, despite a damped and delayed hydrograph response to precipitation and low F_{new} (means of 1.3 to 2.7%). In the weathered bedrock catchments (i.e. dominated by schists and quartzites), rapid infiltration led to large fractions of water that was older than 12 weeks (~ 80%) and very small fractions of water younger than two weeks (~ 3.5%). F_{new} variability with streamflow was near zero, contrasting with the rapid response of the hydrograph to precipitation events. At high specific streamflow, F_{new} was also correlated with bedrock geology and certain land use types. The extensive data set of streamflow $\delta^{18}O$ enabled us to link water storage and release to bedrock geology. Such information is key for a better anticipation of water storage and release functions under changing climate conditions, i.e. long dry spells and high-intensity precipitation events.

1 Introduction

The physical processes that dominate water storage and release are not well understood, causing large uncertainties in predictions for ungauged basins or catchment functioning under a changing climate, i.e. the intensification of the hydrological cycle (Allen and Ingram, 2002; Schaefli et al., 2011; Hrachowitz et al., 2013). The complex interplay of water storage and release processes in the subsurface remain an important knowledge gap which prevents accurate streamflow predictions (Fan et al., 2019). Despite considerable progress gained from hydrological processes research (e.g. Blöschl et al., 2014; Pfister and Kirchner, 2017), we still lack the ability to generalize these findings from instrumented basins to ungauged regions, or from small experimental headwater catchment studies to larger river systems (McDonnell et al., 2007; Schaefli et al., 2011; Fan et al., 2019; Benettin, et al., 2022). Therefore more efforts are needed to investigate how landscape features control the spatial and temporal variability in catchment functions and storage-release processes. To do so we need to move beyond the *status*

quo consisting of detailed characterizations of process heterogeneity and complexity in individual research catchments and instead search for organizing principles underlying the heterogeneity and complexity (Zehe et al., 2014).

Topography and bedrock geology are important factors controlling the magnitude and age of water storage and release in catchments (Creutzfeldt et al., 2014; Sayama et al., 2011; Tromp-Van Meerveld and McDonnell, 2006). Several studies have related these catchment attributes to streamflow generation, e.g. hydrological functioning has been related to bedrock permeability, typically showing that bedrock aquifer storage and release increase with bedrock permeability (e.g. Katsuyama et al., 2005; Uchida et al., 2006; Masaoka et al., 2021; Asano et al., 2022; Weedon et al., 2023). Other tracer-based studies in multiple catchments in Switzerland, Germany, Italy and Austria (Allen et al., 2019; Von Freyberg et al., 2018; Lutz et al., 2018; Gentile et al. 2023; Floriancic et al. 2024) have concluded that elevation, relief, drainage density, quaternary deposits and bedrock geology are important controls on streamflow generation in mountainous environments. In Luxembourg, Pfister et al. (2017) found that the fraction of impermeable bedrock is positively correlated with the standard deviation of isotopic composition of baseflow as well as with the damping of seasonal isotopic cycles between precipitation and streamflow, suggesting shorter transit times in catchments with impermeable bedrock. Similarly Douinot et al. (2022) and Kaplan et al. (2022) have shown slow and delayed streamflow response in catchments characterized by sandstones and more flashy streamflow response in catchments dominated by marls.

Catchment storage and release of water is temporally variable. Currently, little is known about the dominant processes that drive these temporal differences (Kirchner, 2006; Benettin et al., 2022), complicating the quantification of the changing pulse of rivers (Slater and Wilby, 2017, Blöschl et al. 2017). Hence, understanding the non-stationary drivers of streamflow generation remains a key challenge in hydrology. Although computational capabilities and the complexity of numerical models are increasing rapidly (Blöschl et al., 2014), we still fail to capture catchment functioning under unusual conditions, especially extremes (e.g. long-term droughts, extreme flood events). A major reason for this is that catchment functioning is nonstationary and non-linear (e.g. Creutzfeld et al., 2014; Maneta et al., 2018) and the mechanisms generating streamflow – especially during hydrological extreme events – are diverse (Berghuijs et al., 2016). For example the time scales of precipitation reaching the stream vary across the year and with antecedent wetness. Knapp et al. (2019) showed that transit time distributions (TTDs) differ between seasons and with antecedent wetness, while Floriancic et al. (2024) showed that streamflow and soil waters contain slightly more recent precipitation with wetter antecedent conditions. A better understanding of the temporally variable controls of streamflow generation would help to explain temporal variabilities in streamflow magnitude and storage release.

Many field investigations of water storage, transport and mixing processes in the subsurface have relied on input-output relationships of tracer time series. Naturally occurring stable isotopes in water exhibit nearly conservative behaviour (McGuire and McDonnell, 2007), making them powerful tools to assess water ages in streamflow (i.e. transit times of precipitation water through the catchment to reach the stream). The major aim of this study is to leverage measurements of the stable isotope composition of water across multiple catchments to establish relationships between metrics of catchment functioning (i.e. the release of water to streamflow), and landscape attributes (e.g. catchment geological properties). Understanding the physical processes behind streamflow generation is important for realistic hydrological modelling (Seibert and McDonnell, 2015; Schaefli et al., 2011) and improving this understanding depends critically on field observations.

However isotope-based studies have often relied on convolution or sine wave fitting approaches that are not well suited to capture the spatial and temporal heterogeneities that dominate streamflow generation in most catchments (Kirchner, 2016a, b). A common source of bias is *a priori* conjectures concerning the shape of the TTD (Remondi et al., 2018), resulting in, e.g. increasing uncertainty in mean transit time (MTT) estimates when MTT exceeds several years (DeWalle et al., 1997). More recently, calculations of the fraction of young water (Kirchner, 2016b) and transit times extracted from storage selection functions (SAS) (Benettin et al., 2015; Harman, 2015; Rinaldo et al., 2015) have been proposed as more robust methods than traditional MTT estimates. Still SAS functions also rely on unverified assumptions regarding age distributions in catchment storage or evapotranspiration (Kirchner, 2019). The newly developed ensemble hydrograph separation (EHS) technique offers

85 a reduced-assumption alternative, based on the linear regression of tracer concentrations in the stream and lagged concentrations in precipitation across ensembles of rainfall-runoff events (Kirchner, 2019). Young water fractions (Kirchner, 2016b) quantify contributions to streamflow with transit times less than a fixed threshold of ca. 2 to 3 months, but EHS (Kirchner, 2019) is more flexible, quantifying contributions of new water with transit times as short as the interval between stream tracer samples, or any multiple of that sampling interval. Owing to its mathematical formulation, EHS can also be

90 applied to subsets of the tracer time series, e.g. to assess catchment functions under specific conditions or hydrologic extremes (e.g. low flow or high flow events). Following a proof-of-concept study (Knapp et al., 2019), EHS has been used to quantify mobilization of subsurface water in burned and unburned hillslopes in California (Atwood et al., 2023), to estimate new water contributions to tree xylem water in a Peruvian cloud forest (Burt et al., 2023), to identify contrasting catchment release patterns related to hydroclimatic and physical catchment properties across the Austrian and Swiss Alps (Floriancic et al., 2023) and to

95 assess the fractions of recent precipitation in streamflow and at different soil depths along a forested hillslope (Floriancic et al., 2024).

This study investigates the influence of bedrock geology on the time scale of water transport in 12 nested catchments of the Alzette River basin (Luxembourg), a basin where numerous studies on hydrological functioning have been carried out in the past decade (Wrede et al., 2015; Pfister et al., 2017; Douinot et al., 2022; Kaplan et al., 2022). Located at the northern edge of

100 the Paris Sedimentary basin, the geologically diverse Alzette River basin is an ideal setting to test the hypothesis that bedrock geology controls hydrological functioning and the time scales over which precipitation is transformed into streamflow. Our study builds on extensive long-term hydrometric and isotope time series, including up to 13 years of fortnightly $\delta^{18}O$ records in 12 nested catchments. We use EHS to *i)* assess how precipitation intensity affects streamflow and transit times across multiple nested catchments, and *ii)* explore whether fast transit times are specific types of bedrock geology.

105 **2 Methods**

2.1 Physiographic characterisation of the nested catchments

The Alzette River basin, at the northern edge of the Paris Sedimentary Basin, spans a wide range of physiographic settings, making it suitable for studying differences in catchment functioning in contrasting nested headwater catchments. Luxembourg is dominated by schists in the north (*Oesling*) and sedimentary bedrock (marls, calcareous rocks, and sandstone) in the south

110 (*Gutland*) (Fig.1). The northern tip of the study basin belongs to the schistose Ardennes Massif, an elevated plateau (averaging 450 m a.s.l.), where streams are incised, forming relatively steep slopes covered by forests (dominated by oak, beech, and spruce), whereas the plateaus are mainly covered by grassland and cropland. In the remaining part of the basin, sandstone and limestone lithologies are mainly covered by forests, while the marl and claystone catchments are mainly covered by cropland or grassland. Three of the 12 nested catchments have been intensively monitored since 2000 (Wrede et al., 2015): the

115 Weierbach (0.45 km²), Wollefsbach (4.5 km²), and Huewelerbach (2.7 km²). These three catchments have been investigated in detail in previous studies (Wrede et al., 2015; Martínez-Carreras et al., 2016; Pfister et al., 2017; Douinot et al., 2022; Kaplan et al., 2022) and we rely on these in-depth catchment descriptions to infer the behaviour and characteristics of the other nine catchments in similar geologic settings:

The ***Weierbach*** is a steep, forested catchment in the schistose Ardennes massif with elevation ranges from 422 to 512 m a.s.l.

120 It has been monitored and sampled for more than 20 years mainly for eco-hydrological studies (Hissler et al., 2021). The bedrock has generally low porosity, with higher porosities in cracks and fissures. The Weierbach catchment is covered by loamy soils formed from weathered regolith and periglacial deposits, filling the bedrock cracks and fissures and creating substantial subsurface storage volumes. High degrees of weathering and deep root structures enhance infiltration rates and drainage along preferential flow paths, which explains the dominance of subsurface flow in saprolite and periglacial deposits

125 (Angermann et al., 2017). Another characteristic of the catchment is the seasonal difference in streamflow response to

precipitation. In summer, streamflow reacts concomitant with rainfall, while in winter there are typically two peaks, one immediately in response to a precipitation event and a second delayed streamflow peak occurring several hours to days after the event (Martínez-Carreras et al., 2016; Pfister et al., 2023).
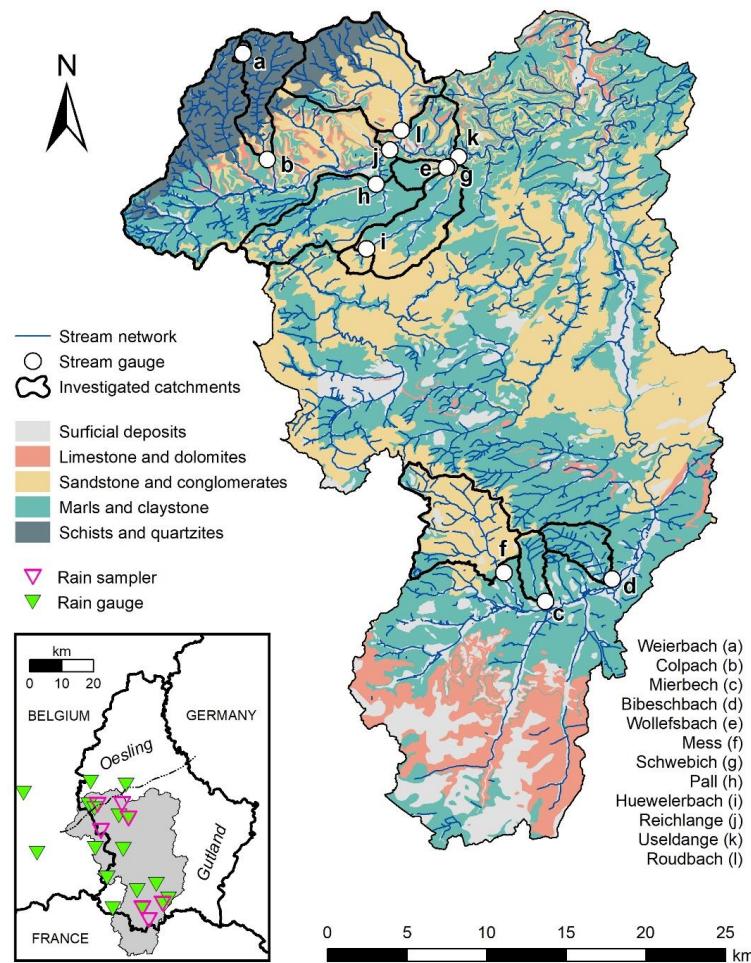
130

Figure 1: Large map: geologic context of the Alzette River basin with the stream network, the outline of the catchment boundaries of the nested catchments, and the location of the stream gauges. Box: extent of the Alzette River basin (grey shaded area) relative to the outline of Luxembourg, Belgium and France (grey lines), and locations of the rain samplers (for isotopic measurements) and rain gauges. Stream samples were taken next to the stream gauges. Geological maps of Luxembourg and the study area were provided by the Luxembourgish geological survey (APC, 2022), and other sources for areas of the Alzette River basin outside of the Luxembourgish boundaries (Hellebrand et al., 2007; BRGM, 2020). The lithology was simplified by regrouping geologies with similar properties for the hydrological characterisation of the catchments (Nijzink et al., 2024).

135

The **Wollefsbach** catchment is formed by alternating layers of marl, sandstone, and limestone inclined southwards (Wrede et al., 2015). The upstream section of the Wollefsbach is dominated by mostly impermeable sandy marls. The gently undulating landscape with elevation ranging from 245 to 306 m a.s.l. is dominated by croplands and pastures, with a dense drainage network that was artificially expanded to avoid cropland waterlogging. The loamy soils, with generally low permeability, have

140

4

macropores from cracks that become established during extended summer dry spells. Macropores of biogenic origin are widespread in spring and autumn because of high earthworm abundance, but are partly disconnected by ploughing, shrinking

145 and swelling of the soils. The seasonal changes in dominant runoff generation processes (i.e. overland flow, shallow subsurface flow in cracks and macropores), in combination with the dense artificial subsurface drainage networks, ultimately lead to a flashy runoff regime (Loritz et al., 2017).

The *Huewelerbach* catchment is typical for the Luxembourg sandstone cuesta landscape, lying on top of a sloped marly bedrock formation (Pfister et al., 2018). Thus alternating layers of porous sandstone and calcareous sandstone are found on the

150 plateaus and on top of the hillslopes, while alternations of marls and limestone emerge in the low parts of the hillslopes and in sections of the valleys close to the stream. The alternation of highly permeable sandstone and, in comparison, less permeable calcareous sandstone layers results in a heterogeneous, yet high, hydraulic conductivity (on mean, 5×10^5 m s^{-1}; Gourdol et al., 2024). The catchment is dominated by a steep central valley with elevation ranging from 280 to 400 m a.s.l., is forested on the plateaus and hillslopes and is covered by grasslands on the foot slopes. The sandy, highly permeable soils prevent surface

155 runoff in large parts of the catchment, except for some downstream sections of the valley that are underlain by marls. The permeable sandstone lying on top of the much less permeable layer of marls provides large aquifer storage with a seasonally constant groundwater flow feeding the perennial springs located at the interface between the two layers (Fenicia et al., 2014). The other nine nested catchments in our study area range in size from 4.4 km^2 to 247.5 km^2 and have similar geologies compared to the Weierbach, Huewelerbach, and Wollefsbach catchments. We grouped the catchments into four hydro-

160 lithological categories, depending on bedrock geology, the related permeabilities, hydraulic conductivity and storage capacity (see Table 1):

    i.   *Weathered layer catchments* (type Weierbach): Shallow weathered regolith on top of fractured bedrock (e.g. schists and quartzites) in steep terrain, with substantial storage capacity (i.e.i.e. Colpach catchment, 19.2 km^2). The river network is dense and concentrated near the valley bottom (Fig. 1), displaying both the high infiltration capacity of

165   the shallow weathered layer on the plateaus and hillslopes, and the impermeability of the bedrock.

    ii.   *Impermeable layer catchments* (type Wollefsbach): Impermeable bedrock (e.g. marls and claystone) with clayey soils, locally sandy facies, limited storage capacities and preferential flow paths, which are reflected by the dense river network (Fig. 1). This category includes the Mierbech (6.8 km^2) and the Bibeschbach (10.6 km^2) catchments. Despite being a sandstone catchment (Fig.1), the Mess (32.2 km^2) is also attributed to this category. The marly

170   sandstone (with sandy claystone) of the Mess has favoured the development of a dense river network that is more characteristic of the impermeable bedrock geologies than permeable ones (e.g. sandstone and conglomerates).

    iii.   *Permeable layer interface catchments* (type Huewelerbach): permeable bedrock (e.g. sandstone and conglomerates) of decreasing thickness towards the valleys with emergence of the underlying less permeable layer (e.g. marls and claystone). These catchments have large storage capacities, with springs and a less dense river network with

175   streamflow generation at the interface between the permeable and impermeable layer. This category includes the Pall (33 km^2) and Schwebich (30.1 km^2) catchments.

    iv.   *Aggregated catchments*: Upstream schistose and quartzite geologies are gradually replaced by sandstone and conglomerates or marls and claystone downstream leading to differences between upstream and downstream streamflow generation processes. This category includes the Roudbach (44 km^2) catchment and the larger Attert River

180   basin subcatchments with gauges at Reichlange (159.5 km^2) and Useldange (247.5 km^2).

Table 1: Catchment area, mean elevation, fraction of major land use types (forest, grassland, agriculture), fraction of bedrock geology types (limestone, sandstone or conglomerates, marls or claystone and schists or quartzites) and fraction of alluvial deposit cover for each of the 12 sub-catchments of the Alzette River basin, extracted from the CAMELS-LUX database (Nijzink et al., 2024).

185 **The hydro-lithological categories given in the last column are as follows: weathered layer (WL), impermeable layer (IL), permeable layer interface (PLI), aggregated (AG) catchments.**

Station	Area [km²]	Elevation [m asl.]	Forest [%]	Grassland [%]	Agriculture [%]	Limestone [%]	Sandstone [%]	Marls [%]	Schists [%]	Alluvial [%]	Categories
a Weierbach	0.5	497	95.6	0.0	0.0	0.0	0.0	0.0	97.4	2.6	WL
b Colpach	19.2	442	51.0	24.0	23.0	5.0	1.0	10.0	81.0	3.0	WL
c Mierbech	6.8	310	34.9	29.1	30.0	0.0	6.1	85.1	0.0	8.7	IL
d Bibeschbach	10.6	298	49.5	22.4	18.5	0.0	0.3	90.1	0.0	9.5	IL
e Wollefsbach	4.4	279	7.1	51.3	38.7	0.6	10.7	81.8	0.0	6.9	IL
f Mess	32.2	325	12.2	41.5	33.2	0.0	75.7	12.7	0.0	11.6	IL
g Schwebich	30.1	297	30.6	40.1	23.6	0.3	33.5	56.3	0.0	9.9	PLI
h Pall	33.0	310	22.7	43.6	26.3	0.0	24.6	64.3	0.0	11.1	PLI
i Huewelerbach	2.7	353	89.6	5.7	0.1	0.0	81.5	11.8	0.0	6.7	PLI
j Reichlange	159.5	357	31.8	30.5	30.8	5.3	18.1	40.6	27.8	8.2	AG
k Useldange	247.5	353	31.5	30.1	31.2	4.9	26.2	36.8	23.9	8.2	AG
l Roudbach	44.0	396	36.0	20.5	35.3	3.4	49.3	8.2	33.3	5.7	AG

2.2 Hydrometric variables in the nested catchments

Our experimental set-up consisted of 12 river gauges and 16 rain gauges (Fig. 1). Hourly precipitation measurements from the LIST monitoring platform were obtained from June 2011 to March 2023 and spatially interpolated separately between the northern (n = 10) and southern stations (n = 7), using ordinary Kriging (*fit.variogram* and *krige* functions, *gstat* package in R; Pebesma, 2004; Gräler et al., 2016). Hourly specific streamflow measurements were also obtained from the LIST monitoring platform from June 2011 to March 2023. We took hourly specific streamflow to calculate daily mean values, taking the 24 hours preceding grab samples in the streams. Some time series were however not continuous due to technical issues. The summer 2021 flood event destroyed the Reichlange station, while the relationship between stage and streamflow changed at Mess and Pall due to changes in river morphology. These missing streamflow values (a total of 622 missing values across all 12 stations out of 56.152 values in total) were interpolated as follows: at each station, we calculated the long-term mean for each day of the year and the ratio between the daily long-term mean and the actual value. To estimate the missing streamflow at a station, we used the ratio from neighbouring stations and multiplied it with the daily long-term mean. Monthly potential evapotranspiration (PET) was obtained using the Thornthwaite (1948) approach from monthly air temperature and day length, as per Pfister et al. (2017).

Our dataset covers 13 years of hydrological observation, encompassing extremely wet (e.g. floods in January 2011, May 2013 and July 2021) and dry time intervals (e.g. spring drought 2011; Fig. 2) and some of the warmest years on record (2011, 2017, 2018, 2019, 2020 and 2021 broke monthly temperature records, MeteoLux (https://www.meteolux.lu/fr/climat/normales-et-extremes/), accessed on 14/03/2025). The study area is characterised by a precipitation gradient from northwest to southeast, typical for the region (Pfister et al., 2004), with annual precipitation (P_a) ranging from 714 mm in the Bibeschbach catchment to 913 mm near Reichlange (Table 2). Precipitation was rather evenly distributed across the seasons, typically with highest totals in winter (265 mm ± 74 mm), similar totals in summer and autumn (206 mm ± 65 mm and 198 mm ± 71 mm, respectively) and lowest totals in spring (154 mm ± 54 mm). Annual potential evapotranspiration (PET_a) varied little between catchments,

210 ranging from 607 to 667 mm and showed pronounced seasonality. Potential evapotranspiration totals were typically highest in summer (272 mm ± 70 mm), similar in spring and autumn (148 mm ± 39 mm and 123 mm ± 32 mm, respectively) and lowest in winter (61 mm ± 16 mm).

2.3 Calculation of storage dynamics

215 We used precipitation, streamflow and potential evapotranspiration (PET) values to calculate catchment storage $S(t)$ in mm as per Pfister et al. (2017):

$$S(t) = [R(t) - Q(t) - \alpha E(t)] + S(t-1), \tag{1}$$
$$if\ S(t-1) < 200\ mm, \alpha = S(t-1)/200$$
$$if\ S(t-1) > 200\ mm, \alpha = 1$$

220 where $S(t)$ is catchment storage (in mm) at day t, $R(t)$ daily precipitation (mm d^{-1}), $Q(t)$ is daily streamflow (mm d^{-1}), $E(t)$ is daily PET (mm d^{-1}), and α is a weighting coefficient for limiting $E(t)$ with decreasing water availability. Daily PET was obtained by dividing the monthly PET by the numbers of days inside a month, described as a suitable approximation in Pfister et al. (2017). For the weighing factor α we assume that field capacity is reached at a catchment storage threshold of 200 mm. We estimated the maximum storage capacity (S_{max}) for each catchment, defined as the highest 0.5 % of daily catchment storage

225 values and computed the storage deficit $D(t)$, as follows:

$$D(t) = S_{max} - S(t). \tag{2}$$

In some cases, the exact water balance was difficult to estimate, because catchments delineated based on topographic criteria might not be entirely representative of the actual drainage area, notably when the topographic boundaries of the aquiclude layer do not exactly follow surface topography. Closing the water balance in the Huewelerbach additionally required

230 accounting for water withdrawn for drinking water from springs in the catchment, on top of likely subsurface flow out of the catchment due to tilting of the geological layers. To approximate these, we assumed a constant loss of 0.4 mm d^{-1} to match the lower end of runoff ratios in the other catchments ($R_c = 0.35$).

2.4 Stable water isotope sampling

235 Cumulative precipitation was sampled every 2 weeks for analysis of the stable isotope composition at four rain gauges in the northern part and three rain gauges in the southern part of the study area (Fig. 1). Similarly fortnightly grab samples of streamflow were taken at the outlet of each of the 12 nested catchments between June 2011 and March 2023. All precipitation and streamflow samples were analysed for δ^{18}O and δ^{2}H using an off-axis integrated cavity output laser spectrometer (Los Gatos TIWA-45-EP, OA-ICOS). Values are reported in per mil notation relative to the Vienna Standard Mean Ocean Water 2

240 standard (VSMOW2) (IAEA, 2017) with a nominal accuracy of 0.2 ‰ for δ^{18}O and 0.5 ‰ for δ^{2}H. Due to gaps in the times series or delayed sampling, the sampling interval was not strictly 14 days, but ~16 days across the entire time series. If intervals between two samplings were longer than 1 month (30 days), they were excluded from the EHS analyses. Samples with precipitation below 0.5 mm were also removed from the analyses.

2.5 Ensemble hydrograph separation and fractions of new water

245 We used the hydrometric and isotope time series to calculate the fraction of new water (F_{new}) in each sample with the ensemble hydrograph separation (EHS) method introduced by Kirchner (2019). EHS estimates the mean contribution of precipitation that becomes streamflow within a time scale defined by the sampling interval. Here the sampling interval is approximately 16 days, thus EHS estimates how much water is younger than ~16 days. In classical hydrograph separation, $F_{new,j}$ is a simple

250   expression of differences in tracer concentrations in streamflow before the event, precipitation (or event water), and streamflow

during the event, based on a simple mass balance (Pinder and Jones, 1969; Rodhe, 1987):

$$F_{new,j} = \frac{C_{Q,j} - C_{Q,j-1}}{C_{P,j} - C_{Q,j-1}},$$ (3)

where $C_{Q,j}$, $C_{Q,j-1}$ and $C_{P,j}$ are the tracer concentrations in the stream after, before, and the event water (i.e.i.e. precipitation).

The underlying idea of EHS is that Equation 3 can also be expressed as a linear regression, where F_{new} is the regression slope

255   in a scatterplot of $C_{Q,j}$ - $C_{Q,j-1}$ versus $C_{P,j}$ - $C_{Q,j-1}$ over the ensemble of observations j (Kirchner, 2019):

$$C_{Q,j} - C_{Q,j-1} = F_{new}(C_{P,j} - C_{Q,j-1}) + \alpha + \varepsilon_j,$$ (4)

where α is the regression intercept and ε_j is the error term. The major difference here is that F_{new} is now a constant, being the

average $F_{new,j}$ which varies with time. An extensive analysis conducted by Kirchner (2019) concluded that a good estimate of

the ensemble F_{new} is:

260    $$F_{new} = \frac{cov(C_{P,j} - C_{Q,j-1}, \ C_{Q,j} - C_{Q,j-1})}{var(C_{Q,j} - C_{Q,j-1})}.$$ (5)

Next, contributions of precipitation to streamflow can be estimated over a range of lag times k, with a maximum lag time m,

to resolve the transit time distribution (TTD) in the catchment. Eventually one is left with an expression analogous to Equation

4:

$$C_{Q,j} - C_{Q,j-m-1} = \sum_{k=0}^{m} \beta_k (C_{P,j-k} - C_{Q,j-m-1}) + \alpha + \varepsilon_j,$$ (6)

265   where β_k is the fraction of streamflow exiting at time j and that had entered k time steps earlier. The regression estimates of β_k

can then be used to estimate the TTD, with the solution provided in Kirchner (2019).

Note that the calculation of F_{new} per se excludes rainless days, and that they need to be separately accounted for using a

correction factor. Scripts in R and Matlab provided by Kirchner and Knapp (2020) allowed us to calculate how much of

streamflow is younger than ~16 days. The F_{new} results presented here are based on the robust estimation algorithm of Kirchner

270   and Knapp (2020) and are not weighted by streamflow amount.

3 Results

3.1 Storage-release dynamics

Although annual precipitation totals were similar across the entire Alzette River basin and roughly distributed evenly across

seasons, streamflow was much more variable across the 12 nested catchments, as reflected in the hydrographs and flow

275   duration curves (FDCs, Fig. 2). The specific streamflow shows clear seasonality with alternating dry summers and wet winters,

following the seasonal variation of evapotranspiration. The seasonality in specific streamflow was less pronounced in the

Roudbach and particularly weak in the Huewelerbach catchment (Fig. 2). While zero-flow conditions frequently occurred in

the impermeable layer or weathered layer catchments, specific streamflow in the other catchments was rarely below ~ 0.1 mm

d^{-1}. The interannual variability also appeared to be more pronounced in catchments that run occasionally dry than in catchments

280   with perennial flow. Overall, catchments with similar geologies had similar FDCs.

Mean annual specific streamflow (q_a) was highest in the weathered layer catchments (Weierbach: 459 mm, Colpach: 453 mm),

followed by the Attert at Useldange (426 mm) and Attert at Reichlange (415 mm) (Table 2). Mean annual specific streamflow

in the Mess ($q_a = 346$ mm), dominated by marly sandstones, was much higher than in the other impermeable layer catchments

(mean q_a ~ 250 mm). Mean annual specific streamflow of the Huewelerbach was the lowest, 161 mm. Annual streamflow

285   totals in all nested catchments were dominated by high winter streamflow, with ratios of summer to winter streamflow $Q_{S/W}$

ranging from 0.21 to 0.38 (Table 2). An exception to this was the Huewelerbach catchment, where summer streamflow was

only ~ 30% lower than winter streamflow ($Q_{S/W} = 0.70$).

Table 2: Hydrometric characteristics for the 12 nested catchments in the Alzette River basin: sampling start and end, annual specific
290 **streamflow, precipitation and potential evapotranspiration (q_a, P_a and E_a, respectively), maximum storage capacity (S_{max}), runoff coefficient (R_c), highest 0.5 percentile of hourly specific streamflow ($q_{99.5}$), and ratio of summer versus winter streamflow ($Q_{S/W}$).**

| Station	Start	End	q_a [mm]	P_a [mm]	E_a [mm]	S_{max} [mm]	R_c [-]	$q_{99.5}$ [mm h^{-1}]	$Q_{S/W}$ [-]
a Weierbach	01/01/2010	30/08/2023	459	865	607	197	0.52	0.55	0.25
b Colpach	01/01/2010	05/01/2023	453	885	642	173	0.51	0.48	0.23
c Mierbech	01/01/2010	17/01/2023	243	736	657	192	0.34	0.50	0.21
d Bibeschbach	01/01/2010	03/01/2023	254	714	657	180	0.36	0.50	0.32
e Wollefsbach	01/01/2010	09/01/2023	257	748	642	145	0.34	0.61	0.22
f Mess	01/01/2010	14/02/2022	346	745	667	154	0.43	0.65	0.26
g Schwebich	01/01/2010	09/01/2023	282	786	642	191	0.36	0.47	0.34
h Pall	01/01/2010	31/01/2022	378	905	642	243	0.40	0.54	0.34
i Huewelerbach	01/01/2010	04/01/2023	161	882	642	433	0.19	0.09	0.70
j Reichlange	01/01/2010	01/01/2021	415	913	641	197	0.45	0.47	0.30
k Useldange	01/01/2010	09/01/2023	426	867	641	171	0.49	0.42	0.33
l Roudbach	01/01/2010	09/01/2023	336	847	625	237	0.40	0.23	0.38

The largest peak hourly specific streamflow on record was in the Mess catchment ($q_{99.5}$ = 0.65 mm h^{-1}), followed by the Wollefsbach ($q_{99.5}$ = 0.61 mm h^{-1}, Table 2). In the weathered layer and impermeable layer catchments, peak streamflow ranged
295 from 0.48 mm h^{-1} to 0.65 mm h^{-1}. Peak streamflow was slightly lower at the Attert gauges (Reichlange and Useldange), and much lower in the Roudbach ($q_{99.5}$ = 0.23 mm h^{-1}), all combined in the aggregated catchment category. Comparing the permeable layer interface catchments, peak streamflow from the Pall was 0.54 mm h^{-1}, comparable to the Schwebich ($q_{99.5}$ = 0.47 mm h^{-1}), in contrast to the Huewelerbach, where peak streamflow was much lower ($q_{99.5}$ = 0.09 mm h^{-1}). Peak streamflow in all catchments was well synchronised (i.e. the large streamflow events occurred after the same rain events in all catchments),
300 but magnitudes differed (Fig 2) during, e.g. the major flood in July 2021. Mean runoff coefficients (R_c) were typically larger in catchments dominated by less permeable bedrock (Fig. A1). Runoff coefficients were highest in the schistose Weierbach and Colpach catchments and the Attert in Reichlange, Attert in Useldange and the Mess catchments (R_c = 0.45 to 0.52, Table 2). The runoff coefficient in the sandstone-dominated Huewelerbach was by far the lowest (R_c = 0.19).

Maximum storage capacity (S_{max}) in the nested catchments ranged from 145 mm to 433 mm (Table 2). The highest S_{max} was
305 by far in the Huewelerbach, where the storage deficit (D) also varied the most (Fig. 3 and A2). The next highest S_{max} occurred in the Pall (S_{max} = 243 mm) and the Roudbach (S_{max} = 237 mm), both containing a large percentage of sandstone facies, like the Huewelerbach. The seasonal variance in D of those catchments was also high. In the remaining catchments, S_{max} was similar, typically around 200 mm. We also observed seasonal variations of D (Fig. A2), with storage close to the calculated maximum during winter, when streamflow was typically higher. Although there was a clear negative relationship between
310 streamflow and storage deficit, there were also examples of high streamflow during times with large storage deficits, especially in the impermeable layer catchments, e.g. in the summer of 2013 in the Mierbech, Bibeschbach and Mess catchments.
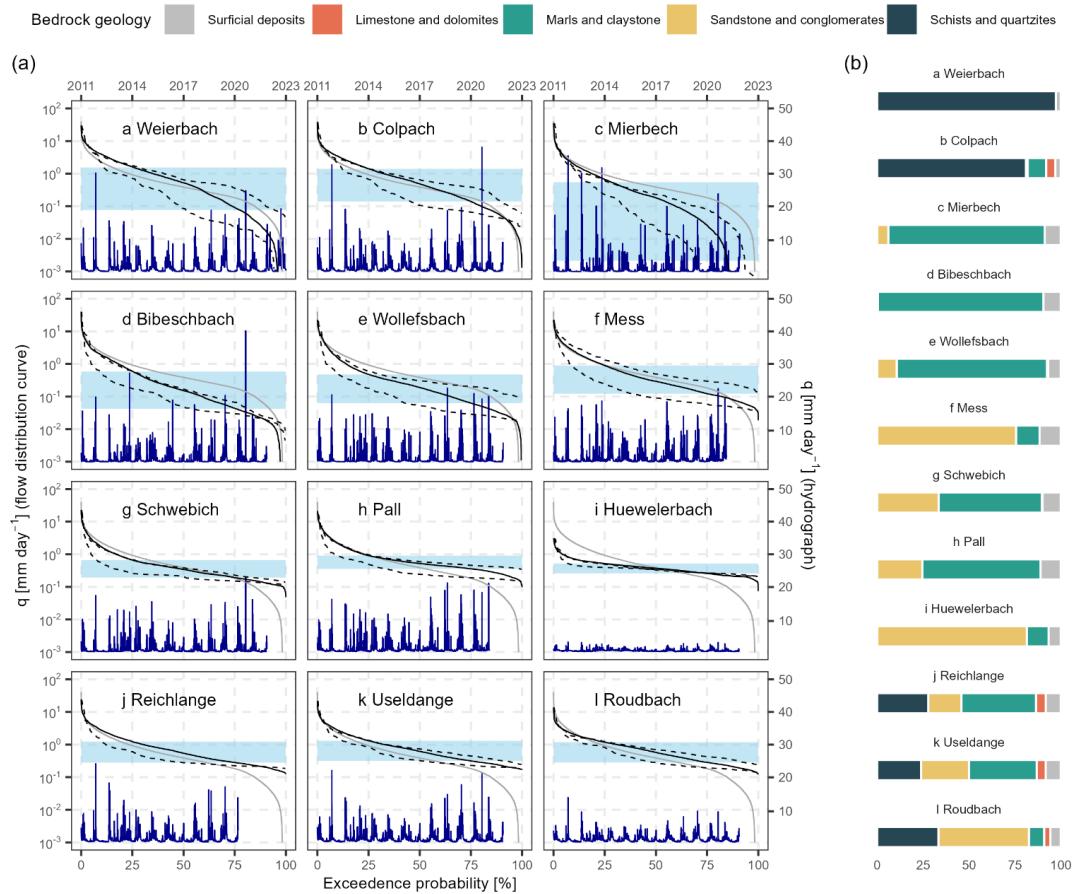
Figure 2: (a) Flow duration curves (FDCs – left y axis (log scale), bottom x axis) and hydrographs (right y axis, top x axis) for the 12
315   **nested catchments. Grey lines represent the mean FDC for the entire Alzette River basin, while solid black lines represent the mean FDCs calculated using the full specific streamflow time series in the individual catchments. FDCs of some individual years are shown to highlight exceptional years (2011, lower dashed line, and 2021, upper dashed line; missing for the Reichlange catchment). The interquartile range (IQR) of the daily specific streamflow in the individual catchments is indicated in light blue shading. (b) Fraction of bedrock geology types in the individual catchments. The results show highly contrasting streamflow behaviours between**
320   **catchments of different bedrock geologies, with overall smaller streamflow variation in catchments consisting of a larger fraction of sandstone and conglomerates.**
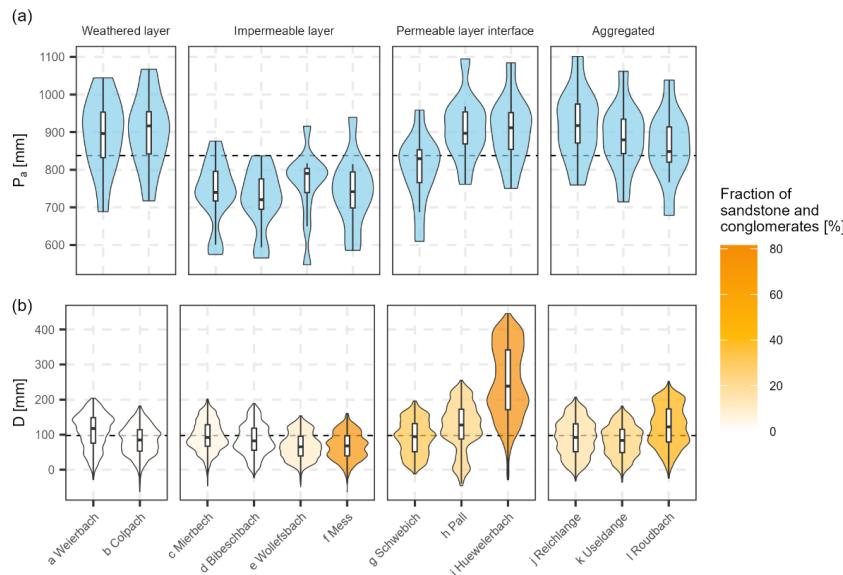
Figure 3: Violin plots and boxplots of (a) annual precipitation (P_a) and (b) daily storage deficit (D) in the 12 nested catchments. The dashed horizontal lines represent the medians across all catchments for reference. Annual precipitation is similar across the catchments, differences exist according to the location of the catchments along the northwest to southeast gradient of precipitation totals. The dynamics of storage deficits were of similar range in most catchments, yet larger in catchments with a large fraction of sandstone and conglomerates.

3.2 Isotope variability in fortnightly stream and precipitation measurements

Fortnightly $\delta^{18}O$ of the four stations in the north and the three stations in the south followed similar patterns. Winter $\delta^{18}O$ was lower than in the summer, following the typical seasonality induced by temperature expected at this latitude (Dansgaard, 1964; Feng et al., 2009) (Fig. 4). Median $\delta^{18}O$ varied little between neighbouring stations, with values of -7.3 ‰ and -7.4 ‰ in the north and south, respectively, and all with interquartile ranges around 4.0 ‰.

The amplitude of the seasonal precipitation $\delta^{18}O$ signal was damped in streamflow, with large differences between the different hydro-lithological catchment categories (Fig. 5). Catchments with permeable layer interfaces and large storage volumes (e.g. Huewelerbach) had much smaller seasonal streamflow $\delta^{18}O$ amplitudes compared to the catchments dominated by marly bedrock (and thus less permeable subsurface properties) with limited storage capacity (Fig. 5). Streamflow $\delta^{18}O$ amplitudes were also smaller in weathered layer catchments. Interquartile ranges of $\delta^{18}O$ varied between 0.6 ‰, 0.8 ‰, 0.4 ‰ and 0.4 ‰ for weathered layer, impermeable layer, permeable layer interface and aggregated catchments, respectively. Streamflow $\delta^{18}O$ from catchments with similar bedrock geologies showed similar seasonal amplitudes. Compared with the median-weighted $\delta^{18}O$ in precipitation, the median weighted streamflow $\delta^{18}O$ were lower in the weathered layer (-8.4 ‰), aggregated (-7.9 ‰) and permeable layer interface catchments (-7.9 ‰). However in the impermeable layer catchments, median-weighted streamflow $\delta^{18}O$ (-7.4 ‰) were closer to the median-weighted $\delta^{18}O$ in precipitation. Streamflow $\delta^{18}O$ in catchments from all hydro-lithological categories were occasionally affected by strong rainfall, with pronounced deviations from the typical streamflow $\delta^{18}O$ (Fig. 5a).
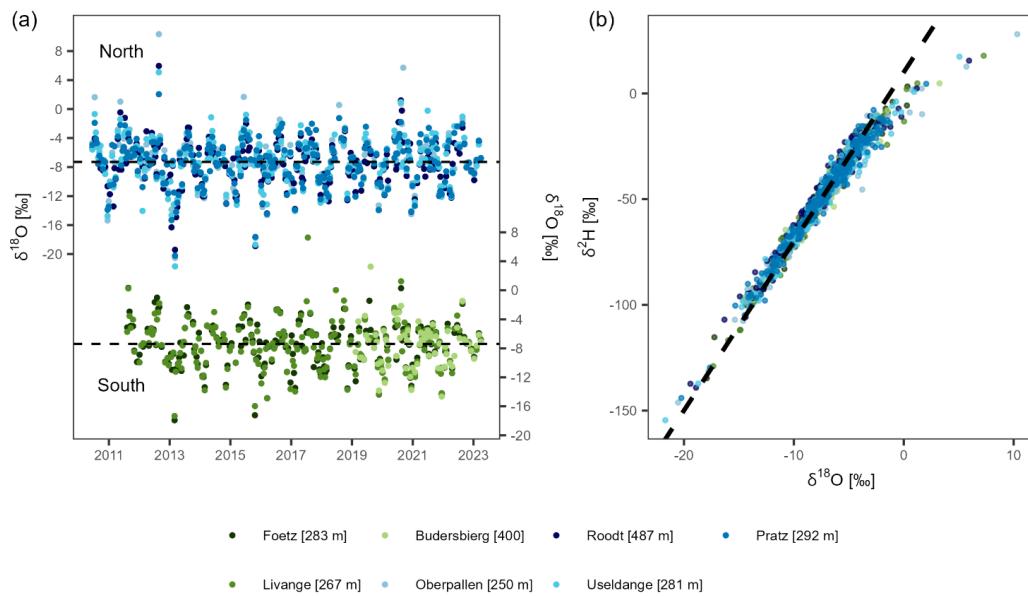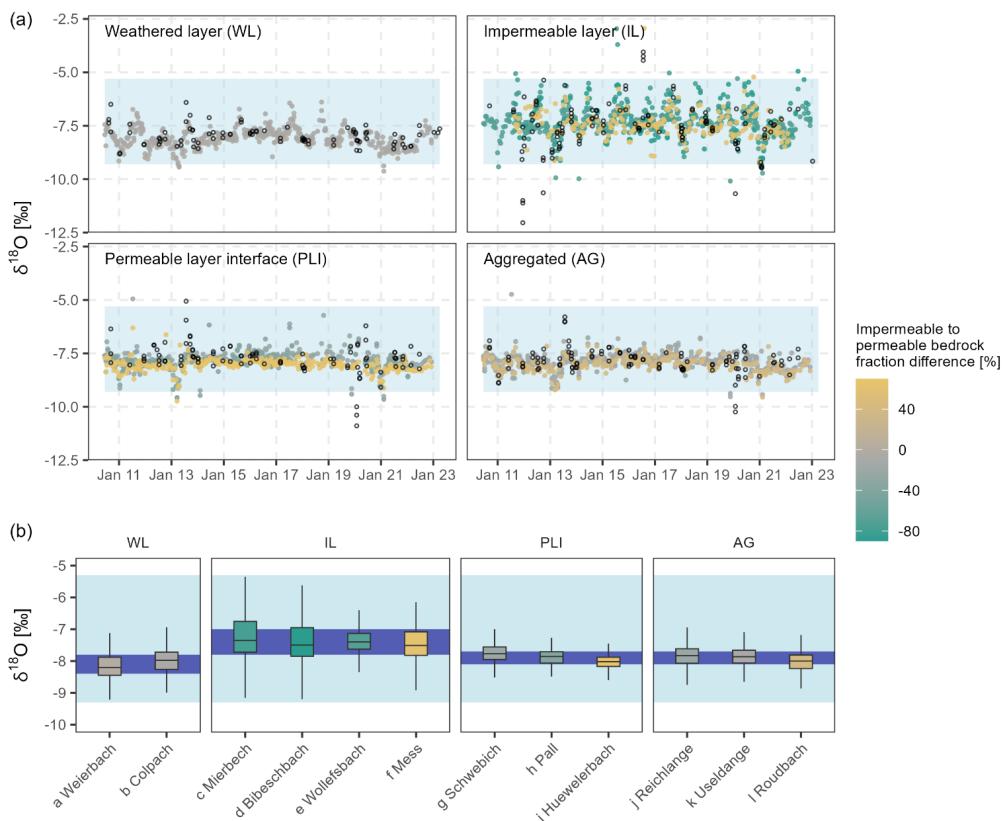
11

Figure 4: (a) Oxygen stable isotope composition of fortnightly precipitation samples of the seven rain gauges between 2011 and 2023.
350 **(b) Dual isotope plot (oxygen and hydrogen) and boxplots of the isotope composition at the seven rain gauges. The dashed line indicates the Global Meteoric Water Line (GMWL) with the equation δ²H = 10 + 8 × δ¹⁸O.**

Figure 5: (a) Isotope signatures in streamflow from 2011 to 2023 for all 12 nested catchments grouped into hydro-lithological
355 **categories. Samples that were taken after strong rainfall events (i.e. more than 15 mm in the 72 hours preceding the sampling) are indicated by empty circles. (b) Boxplots of δ^{18}O in streamflow in all 12 nested catchments showing catchment-specific differences inside the hydro-lithological categories. The shadings indicate the interquartile range of precipitation (light blue) and streamflow (dark blue), displaying the damping of precipitation δ^{18}O in streamflow. The colour shading corresponds to the difference of the fraction of permeable bedrock (i.e. sandstone and conglomerates) minus the fraction of impermeable bedrock (i.e. marls and**
360 **claystone).**

3.3 Ensemble hydrograph separation
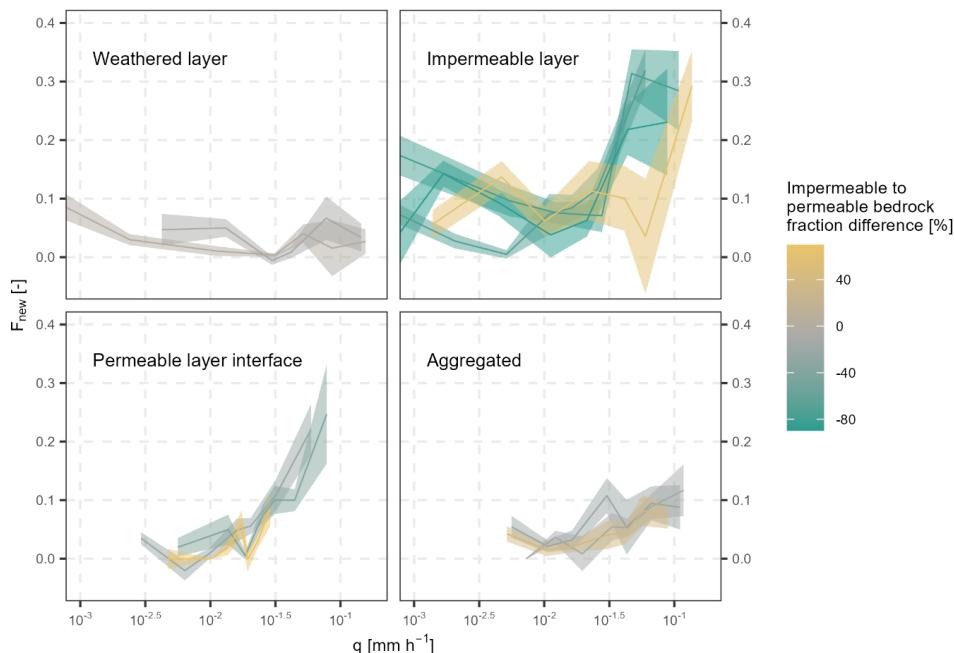
Figure 6: Fraction of water younger than ~ 16 days (F_{new}) in the twelve nested catchments with increasing specific streamflow (taking
365 **the 24-hour means of specific streamflow before the timing of the grab samples) (lines, see Fig. B1 for the exact streamflow quantiles), including the standard errors (shading) regrouped into hydro-lithological categories. Mean F_{new} was largest in the impermeable layer catchments and only substantially increased with higher mean daily specific streamflow in the impermeable layer and permeable layer interface catchments. The colour shading corresponds to the difference of the fraction of permeable bedrock (i.e. sandstone and conglomerates) minus the fraction of impermeable bedrock (i.e. marls and claystone).**

370

The estimated mean fraction of water younger than ~16 days (F_{new}) was largest in the impermeable layer catchments (mean of 8.7%), ranging from 4.5% at Wollefsbach to 8.7% at Mess and 11.9% at Mierbech. (Fig. 6). Mean F_{new} in the remaining catchments did not exceed 4.0%. In the permeable layer interface catchments mean F_{new} were 2.1 % (2.2% at Schwebich, 2.7% at Pall and 1.3% at Huewelerbach); mean F_{new} was 3.3% in the weathered layer catchments and 3.0% in the aggregated

375 catchments.

F_{new} increased with increasing streamflow in most catchments (and with 2-week antecedent precipitation, Fig, B2), except for the weathered layer catchments, where F_{new} tended to be similar independent of streamflow magnitude (Fig. 6). The highest F_{new} was at high streamflow in the Wollefsbach (up to ~ 35%). The impermeable layer catchments showed the greatest increase in F_{new} with increasing streamflow (from a mean of ~ 9 to ~ 30%). In relative terms, increasing F_{new} with increasing precipitation

380 and streamflow was also evident in aggregated catchments (from a mean of ~ 3 to ~ 10%) and, most strikingly, in the permeable layer interface catchments (from a mean of ~ 2 to ~ 25%) (Figures B1 and B2).

We further used the EHS method to estimate TTDs in the 12 nested catchments for longer time intervals. By taking the integral of the obtained TTDs, we were able to estimate F_{new} for different, longer sampling intervals (i.e. time windows from 2 up to 26 weeks, Fig. 7). This analysis revealed that F_{new} increased with the square root of the length of time interval in all catchments,

385 reaching up to ~ 40% after 26 weeks. We also calculated F_{new} for the upper 20% of streamflow and found that these high-flow F_{new} were systematically higher compared to F_{new} for all the streamflow data combined, except in the weathered layer catchments and one aggregated catchment (Roudbach). The difference between F_{new} calculated for overall conditions and high-streamflow conditions also tended to increase at longer intervals, e.g. for the marly sandstone Mess catchment, or the permeable layer interface catchments (but not the Huewelerbach). F_{new} in the Wollefsbach plotted close to the mean of all catchments, contrasting with other impermeable layer catchments, which had substantially higher F_{new} (Fig. 7e). F_{new} for the upper 20% of

390 streamflow increased with the interval length to a mean of $23.4 \pm 3.0\%$ at 26 weeks in the weathered layer catchments, $46.6 \pm 21.4\%$ in the impermeable layer catchments, $18.9 \pm 13.2\%$ in the permeable layer catchments and $20.3 \pm 9.0\%$ in the aggregated catchments.
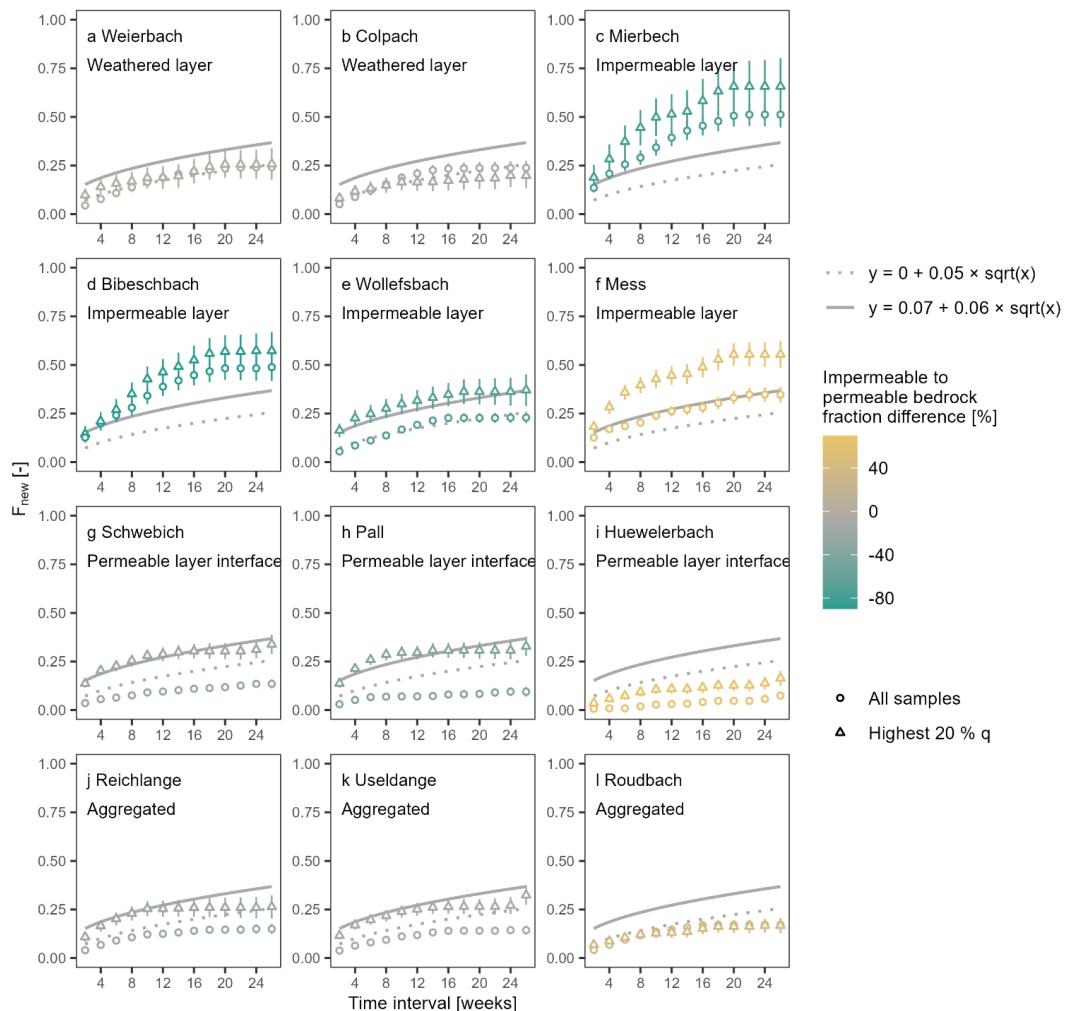

395 **Figure 7: Estimates of fractions of new water (F_{new}) and respective standard errors for sampling intervals of two to 26 weeks. The dotted lines indicate the mean for all 12 catchments based on the entire time series and the continuous lines indicate the mean for all 12 catchments for the highest 20% of specific streamflow; readers should note that these reference lines are the same in all panels. F_{new} increased with increasing interval length and was systematically higher for the highest 20% of specific streamflow (triangles) than for the entire timeseries (circles) in the impermeable layer catchments, two of three aggregated catchments and permeable**

400 **interface layer catchments. The colour shading corresponds to the difference of the fraction of permeable bedrock (i.e. sandstone and conglomerates) minus the fraction of impermeable bedrock (i.e. marls and claystone).**

3.4 Relationship between F_{new} and catchment properties
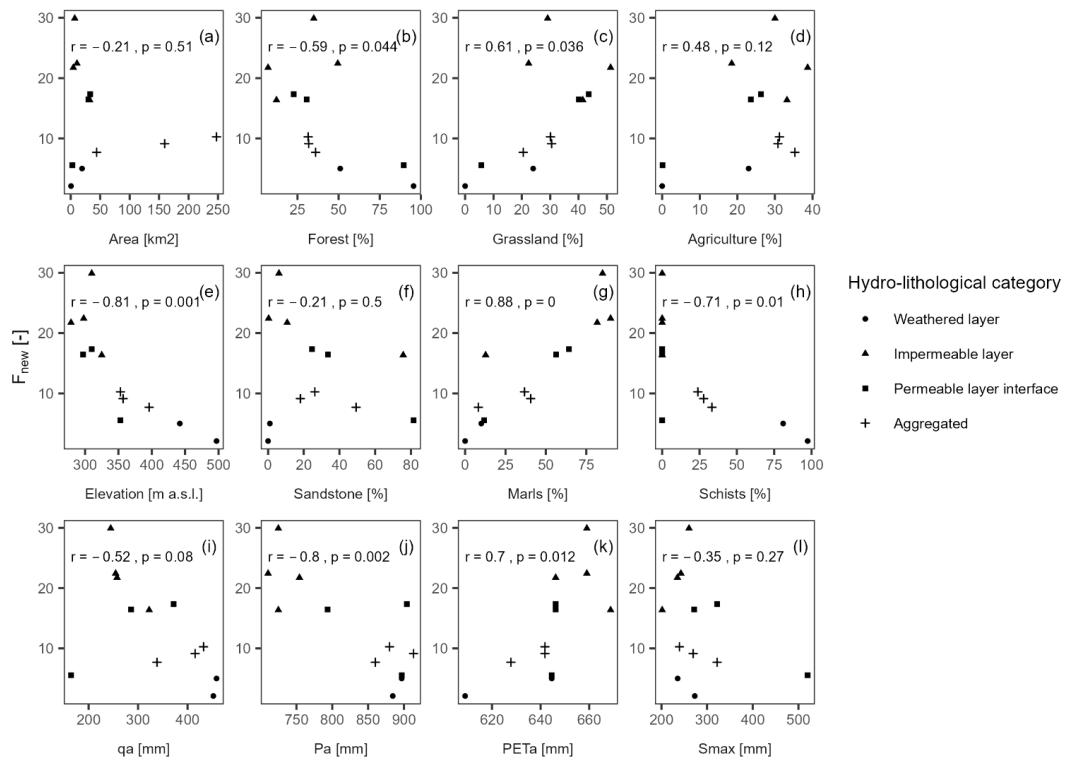
405 **Figure 8: Scatter plots of the fractions of water younger than ~ 16 days (F_{new}) for the highest 20 % of specific streamflow by (a) catchment area, fractions of (b) forest, (c) grassland and (d) agriculture, (e) mean catchment elevation, fractions of (f) sandstone, (g) marls and (h) schists, (i) annual specific streamflow, (j) annual precipitation, (k) annual potential evapo-transpiration, and (l) maximum storage capacity in the 12 catchments. Correlations are expressed in each plot with Pearson's r and corresponding p (rounded after the third decimal). F_{new} exhibited highly significant correlations with mean catchment elevation (p = 0.001) and**
410 **fraction of marls (p < 0.001) for the highest 20% of streamflow. Weaker correlations were found for land use types, fraction of schists, mean annual precipitation, and mean annual potential evapotranspiration. A correlation matrix of the physiographic catchment properties is shown in supplementary figure C1.**

Our results showed links between F_{new} and physiographic catchment attributes. Especially bedrock geology had a substantial

415 effect on the fraction of water younger than ~16 days at high streamflow. F_{new} for the highest 20% of streamflow (Fig. 8) was

positively correlated with fraction of marls (r = 0.88, p = 0.001) and PET_a (r = 0.70, p = 0.012), and negatively correlated with

the mean catchment elevation (r = - 0.81, p-value = 0.001), fraction of schists (r = - 0.71, p = 0.01), and P_a (r = - 0.80, p =

0.002). Weaker correlations were found for land use types, i.e. fractions of forest (r = - 0.59, p = 0.044) and grassland (r =

0.61, p = 0.036). There were no significant relationships between F_{new} and catchment area, fractions of sandstone, mean q_a or

420 S_{max}. However we observed smaller F_{new} variance with increasing catchment size (Fig. 8a). Note that bedrock geology, land

use and catchment elevation were all significantly correlated to each other (Fig. C1).

4 Discussion

4.1 Bedrock geology effects on catchment response, new water fractions, and fast flow paths in nested catchments

Many years of hydrological studies in the Alzette River basin (e.g. Wrede et al., 2015; Martínez-Carreras et al., 2016; Pfister
425   et al., 2017; Douinot et al., 2022; Kaplan et al., 2022) have shown that bedrock geology has large effects on catchment
hydrological behaviour, but the proportion of water travelling to the streams via flow paths with different transit times have
not previously been quantified. Here we demonstrate a clear link between bedrock geology and catchment responses, isotope
signatures and fractions of water younger than ~16 days (F_{new}) in 12 nested catchments of the Alzette River basin. In the
impermeable layer catchments, median-weighted streamflow $\delta^{18}O$ was nearly identical to $\delta^{18}O$ in precipitation (-7.4 ‰)
430   suggesting that streamflow was well mixed between summer and winter precipitation, unlike the other catchment clusters
where streamflow was dominated by winter precipitation. F_{new} was highest in impermeable layer catchments (9.6 to 12.2%)
and increased with higher streamflow in catchments with at least some sections of marly, impermeable bedrock (F_{new} up to
45%, Figs. 6 and B1). This increasing F_{new} behaviour was accordingly observed in permeable layer interface catchments (where
sandstone and conglomerates are gradually replaced by underlying marl and claystone layers), but absent in weathered layer
435   catchments, despite their marked reactivity in streamflow response (Figs. 2 and 6). In weathered layer catchments, over 80%
of the streamflow was older than 12 weeks (or three months), even at high streamflow (Fig. 7). In a similar study in Central
Germany (23 sub-catchments), fractured bedrock (greywacke, schist, and granite) and freely draining soils in mountainous
sub-catchments led to deep flow paths with long transit times, in contrast to rapid drainage with short transit times in the
sedimentary bedrock lowlands (Lutz et al., 2018). The study yielded fractions of young water (water less than 2 to 3 months
440   old) from 1 to 27%, corroborating our results which lie in the same range (Fig. 7).

Other important controls that have been reported to affect catchment functions include topography, precipitation, soil
properties or vegetation (Von Freyberg et al., 2018; Lutz et al., 2018, Floriancic et al., 2023), yet in our study area, many of
these parameters were correlated (Fig. C1) or similar across the different catchments. Across the 12 examined catchments the
underlying bedrock geology played an important role in their shaping landscapes thereby affecting topography, soil properties
445   or vegetation (Troch et al., 2015). Considering only characteristics that were independent from each other, we found that
isotopically inferred F_{new} during times of high streamflow was positively correlated to the percentage of marls (r = 0.88, p =
0.001), and to the percentage of grassland area (r = 0.61, p = 0.036, Fig. 8). The negative correlation with forest area (r = -
0.59, p = 0.044) may also relate to the geological properties, since the two catchments with the highest percentage of forest
area also consist almost exclusively of schist or sandstone, which are generally associated with low F_{new}. One could expect
450   higher infiltration rates with root structures in forest, e.g. as reported in weathered layer catchments (Angermann et al., 2017),
and soil consolidation or artificial drainage in agricultural areas triggering fast overland and shallow subsurface flow (Loritz
et al., 2017), leading to correlations between F_{new} and forest and agriculture land use.

Like previous investigations on physiographic controls on catchment functions, this study also faced uncertainties related to
the spatial heterogeneity in catchment attributes. Geological features of the Alzette River basin are spatially heterogeneous,
455   impeding straightforward attributions to simplified geological units. This was notably the case in the marly sandstones of the
Mess, a catchment attributed to the impermeable layer category (Fig. 5). Flow paths under 2 weeks were only activated at the
highest streamflow, indicating fast infiltration and retention except during high-intensity rainfall (Fig. B2), which contrasts
with the rest of the impermeable layer catchments. Another limitation was that catchments attributed to the same hydro-
lithological category, e.g. permeable layer interface catchments or aggregated catchments, had widely varying percentages of
460   marls and claystone (and reversely, sandstone and conglomerates). Despite the processes being of a similar nature in these
catchments, the "marly" characteristics of flashy streamflow responses and fast flow paths might especially affect catchments
where marls are more represented. This could explain the relatively small effect of increasing streamflow on F_{new} in the
Roudbach, which contains a significantly lower fraction of marls and claystone (and higher fraction of sandstone and

conglomerates) compared to the other aggregated catchments (Fig. B1). Other sources of uncertainty are related to

465 measurements such as rain gauges that are not necessarily always representative of the rainfall over an entire catchment. Also, in the densely populated Alzette River basin anthropogenic infrastructure (e.g. drainage channels in the Wollefsbach or water captured from springs in the Huewelerbach) interferes with natural flow processes.

When discussing transit times, flow paths and F_{new}, it is important to consider the time scales and the definitions of words such as 'new' or 'fast'. F_{new} inherently increases with greater aggregation time intervals used for the calculation, because those

470 determine what counts as 'new'. For any given time scale of 'new' water, F_{new} also reflects the type and geology of the catchment and streamflow (Fig. 7). Since we were working with fortnightly data in this study, and thus F_{new} is the fraction of water less than two weeks old rather than 'event water' from individual precipitation occurrences, high F_{new} is consistent with large pre-event (but relatively recent) water contributions to streamflow. This study describes catchment functions under varying conditions and in different physiographic settings, rather than analysing the streamflow response to individual

475 precipitation events. Still, we could observe that large precipitation events led to occasional rapid responses of the hydrograph (Fig. A2) and isotopes, illustrated by F_{new}, increased with 2-week antecedent precipitation (Fig. B2). This can occur when intense precipitation falls on soils with low infiltration capacities, either because they are saturated or very dry (Loritz et al., 2017).
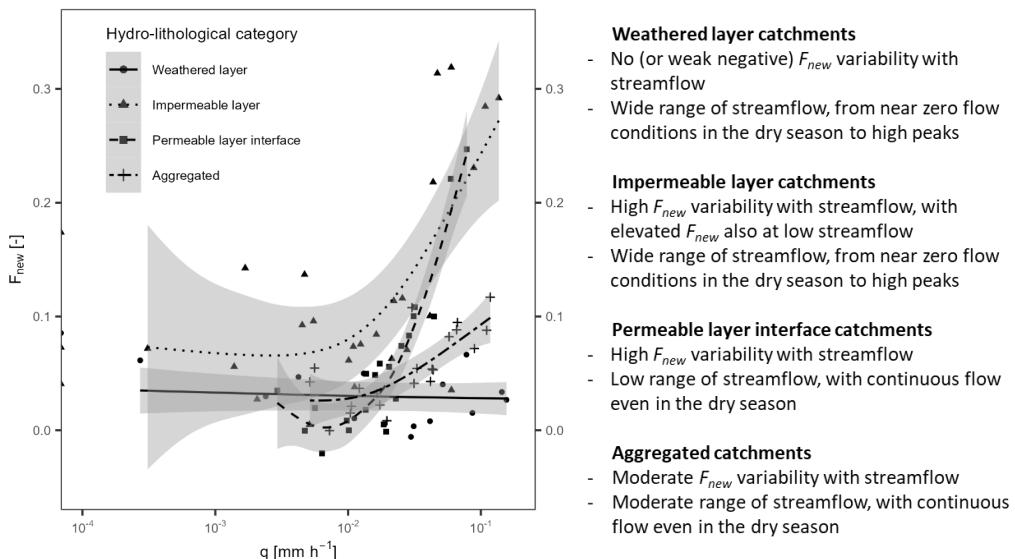
480 **4.2 Conceptualisation of catchment functions across varying streamflow for representative bedrock geologies**

Our finding that a substantial fraction of stream water in weathered layer catchments is many months old, at both high and low flows, highlights the dominance of storage and subsurface flow in the regolith. This occurs as a combination of high infiltration rates together with fast vertical velocities (Glaser et al., 2019; Scaini et al., 2017), resulting from high degrees of weathering in the regolith and deep root structures (Angermann et al., 2017). Fast lateral displacement (Glaser et al., 2019) in the weathered

485 layer eventually leads to a significant fraction of streamflow being less than 12 weeks old (about 20%, see Fig. 7), despite the rest being older water and only a small fraction being less than 2 weeks old (about 3.3%). The retention of event water could additionally be caused by a "fill-and-spill" mechanism (Tromp-Van Meerveld and McDonnell, 2006) in fissures filled by weathered material, explaining the delayed streamflow peak behaviour typical of weathered layer catchments. The schistose catchments in this study are indeed known to frequently shift between single and double peak hydrographs, mostly in response

490 to alternating contributions from various landscape units and the exceedance of storage thresholds (Martínez-Carreras et al., 2016). The first peak was found to be the immediate response to rainfall dominated by flow paths close to the surface. The second, larger peak, taking days to build up, was controlled by delayed precipitation release from storage, e.g. as demonstrated by a sprinkling experiment in the Weierbach (Scaini et al., 2018). The dominant exfiltration of groundwater (Glaser et al., 2016, 2020) even during times of high subsurface storage could possibly explain why mean and high-flow F_{new} are similar

495 (Fig. 7). Such dominant contributions of groundwater might be the reason why we could not find a systematic relationship between F_{new} and streamflow magnitudes. High infiltration rates and substantial retention volumes in the weathered layers of bedrock have also been reported for explaining the somewhat counter-intuitive observation of small F_{new} in higher-elevation catchments with 'impermeable' schistose bedrock formations (Lutz et al., 2018).

Permeable layer interface catchments exhibit deep infiltration of event water, retention of event water in subsurface storage,

500 and slow sub-surface lateral flows at the aquifer-aquiclude interface that eventually reach the stream with a substantial delay, although this delay is shorter for precipitation falling closer to the stream (Pfister et al., 2018). In the permeable layer interface catchments, we found increasing F_{new} with higher streamflow – suggesting the activation of preferential flow paths, and probably also overland or shallow sub-surface flow when the infiltration capacity is exceeded in the lower near-stream section dominated by marly lithologies. In impermeable layer catchments, overland and shallow sub-surface flow dominate, even for

505 small rain events (Douinot et al., 2022). This fast flow path component becomes even more important with the filling of the

limited storage volume in these catchments, translating into high F_{new} reaching the stream. The activation and de-activation of preferential flow paths depending on the volumes of water in storage after the wetting phase in winter, i.e. the "inverse storage effect", has already been reported from numerous other investigations using similar metrics (Von Freyberg et al., 2018; Harman, 2015; Rodriguez et al., 2018). Based on our findings, we propose a summary for how F_{new}, i.e. fast flow paths,

510 variability with streamflow is predominantly controlled by bedrock permeability (Fig. 9).

Weathered layer catchments
- No (or weak negative) F_{new} variability with streamflow
- Wide range of streamflow, from near zero flow conditions in the dry season to high peaks

Impermeable layer catchments
- High F_{new} variability with streamflow, with elevated F_{new} also at low streamflow
- Wide range of streamflow, from near zero flow conditions in the dry season to high peaks

Permeable layer interface catchments
- High F_{new} variability with streamflow
- Low range of streamflow, with continuous flow even in the dry season

Aggregated catchments
- Moderate F_{new} variability with streamflow
- Moderate range of streamflow, with continuous flow even in the dry season

Figure 9: Summary of water younger than ~ 16 days (F_{new}) with increasing specific streamflow in catchments from different hydro-lithological categories. Curves were fitted to F_{new} disregarding the individual catchments, using a generalized additive model (GAM)
515 **fitting algorithm with the *geom_smooth* function in R.**

4.3 Scale effects on time scales of catchment storage-release functions

River basins are intrinsically complex systems, exhibiting considerable spatial and temporal heterogeneity. With the spatial organisation of hydrologic dynamics being constantly (re)shaped by work performed by wetness and vegetation, we often fail

520 to capture the direct controls on the spatial and temporal heterogeneity of catchment functioning and evolution. In this context, rigid and static conceptualisations of catchments may be serious impediments to, e.g. climate mitigation and adaptation measures (Ehret et al., 2014). Despite considerable progress made in transit time estimation with new concepts proposed around time-variant transit and residence times (e.g. Botter et al., 2011; Kirchner, 2016a, b, 2024), upscaling from headwater catchments to mesoscale catchments to large drainage basins remains challenging. Soulsby et al. (2009) and Hrachowitz et al.

525 (2010) found that variation in MTT among 32 Scottish catchments (0.5–1700 km^2) was highest for catchments smaller than 10 km^2 and averaged ~ 2 years. In the Alzette River basin, Pfister et al. (2017) found the highest spread of MTTs for catchments smaller than 20 km^2, with a mean MTT of ~ 1.4 years in the largest catchments.

In the current nested catchment set-up (0.45 to 247.5 km^2), with contrasting physiographic settings and rather homogenous climate, we found that bedrock geology controls fast flow paths. Major geological properties overlap with distinct hydrological

530 functioning. In larger and less homogenous catchments, these patterns tend to converge to a central behaviour, but small areas with discrete bedrock geologies can distinctively affect rainfall-runoff response. For example, fast flow paths activated in comparatively small marly headwaters may still shape the hydrograph further downstream by exceeding contributions from less responsive areas. Likewise contributions from small permeable layer interface headwaters or sandstone sections may help

sustain streamflow during dry spells in larger aggregated catchments (including less permeable and contributory sections).
535   However a presumed variance collapse in F_{new} beyond ~ 150 km^2 (Figs. 6 and 8) suggests that the variability in flow path responses is dampened with increasing catchment size. The variance collapse in F_{new} may also be attributed to the combined expression of increasing basin sizes and aggregated expressions of distinct regional physiographic features and associated flow path configurations.

4.4 Implications of our findings for predictions in ungauged basins and predicting catchment responses under non-
540   **stationary boundary conditions**

For projecting hydrological responses under future climate scenarios and assessing catchment functions under non-stationary conditions, we can rely on the activation of fast flow paths with increasing rainfall intensities and streamflow, which appear to be linked to bedrock geology (Figures 6, B1 and B2). Our results suggest that an intensification of the hydrological cycle
545   (Allen and Ingram, 2002; Blöschl et al., 2017) may lead to the most apparent changes in impermeable layer catchments, and probably significantly affect permeable layer interface catchments with at least some marl and claystone-dominated sections. For our study area, large storage capacities in the sandstone-dominated Huewelerbach catchment and high infiltration capacities in weathered schistose catchments (Angermann et al., 2017) also led to a strong buffering of fast flow paths during highly intense precipitation events, corroborating previous observations in schistose geologies (Lutz et al., 2018). In general,
550   our results validate the mechanistic conceptualisation of fractions of young water (2 to 3 months old) relating to streamflow previously identified in the Swiss Alps, where F_{new} is linked to catchment wetness, infiltration capacity and storage volume (Von Freyberg et al., 2018). The variance collapse in F_{new} (younger than ~ 16 days) for catchments larger than 150 km^2 further illustrates that the transferability and reproducibility of our findings is limited to smaller catchments. Beyond the mesoscale, the variability in flow path responses might become smaller, but it will certainly remain affected by processes occurring in
555   small headwater catchments, as shown by our findings (e.g. F_{new} increasing with higher streamflow in aggregated catchments). Relatively small proportions of distinct bedrock types shape the overall catchment response to precipitation suggesting that more attention should be given to the most distinguishable sections of a catchment, instead of considering only spatially averaged properties across entire catchments.

5 Conclusions

560   With a view to better understand how landscape features translate into catchment functions, driven by non-stationary forcings, we assessed the influence of bedrock geology on isotopically inferred fast flow paths in a set of 12 nested catchments. We found that the fractions of new water (F_{new}; water younger than ~16 days in this study) were linked to bedrock geology. F_{new} was highest (up to ~ 45%) and increased most with streamflow, in impermeable layer catchments (i.e. dominated by marls and claystone), due to dominant overland and shallow sub-surface streamflow contributions. While increasing F_{new} with increasing
565   streamflow was also observed in permeable layer interface catchments (i.e. with high a fraction of sandstone and conglomerates with underlying marl and claystone layers) and linked to the contribution of downstream impermeable layer sections, it was absent from weathered layer catchments (i.e. catchments dominated by schists and quartzites). In weathered layer catchments, a major fraction of water (~ 80%) is older than 12 weeks, with only a small fraction being less than 2 weeks old (F_{new} of ~ 3.5%). For catchments smaller than 150 km^2, our results support the hypothesis that bedrock geology, linked to different
570   storage-release dynamics, translates into quantifiable variations in fractions of fast flow paths inside the catchments. Catchments with similar bedrock geologies showed similar fast flow path patterns evolving with increasing rainfall intensities and streamflow. The contrasting fast flow path behaviour of permeable and impermeable bedrock formations is an important finding for predictions of catchment functions under non-stationary conditions or in ungauged basins. According to our results, an intensification of the hydrological cycle would lead to the most apparent changes in impermeable layer catchments, while

575 also affecting permeable layer interface catchments that have large proportions of marls. The collapse in the variance of F_{new}

for catchments larger than 150 km^2 suggests an averaging effect through the aggregation of contrasted responses from different

contributing areas. Sandstone catchments with large storage capacities and weathered layer catchments with high degrees of

weathering showed only small contributions of fast flow paths to streamflow. These findings corroborate other inter-catchment

studies in different settings and climates, suggesting that catchment sensitivity to a changing climate can be inferred from

580 landscape features. Success will depend on our ability to produce appropriately simplified geological maps adapted for

hydrological applications at the macroscale and to provide an alternative to the currently limited hydrometric datasets. An

effort needs to be made to identify the controlling parameters or characteristics to produce such maps.

Appendix A
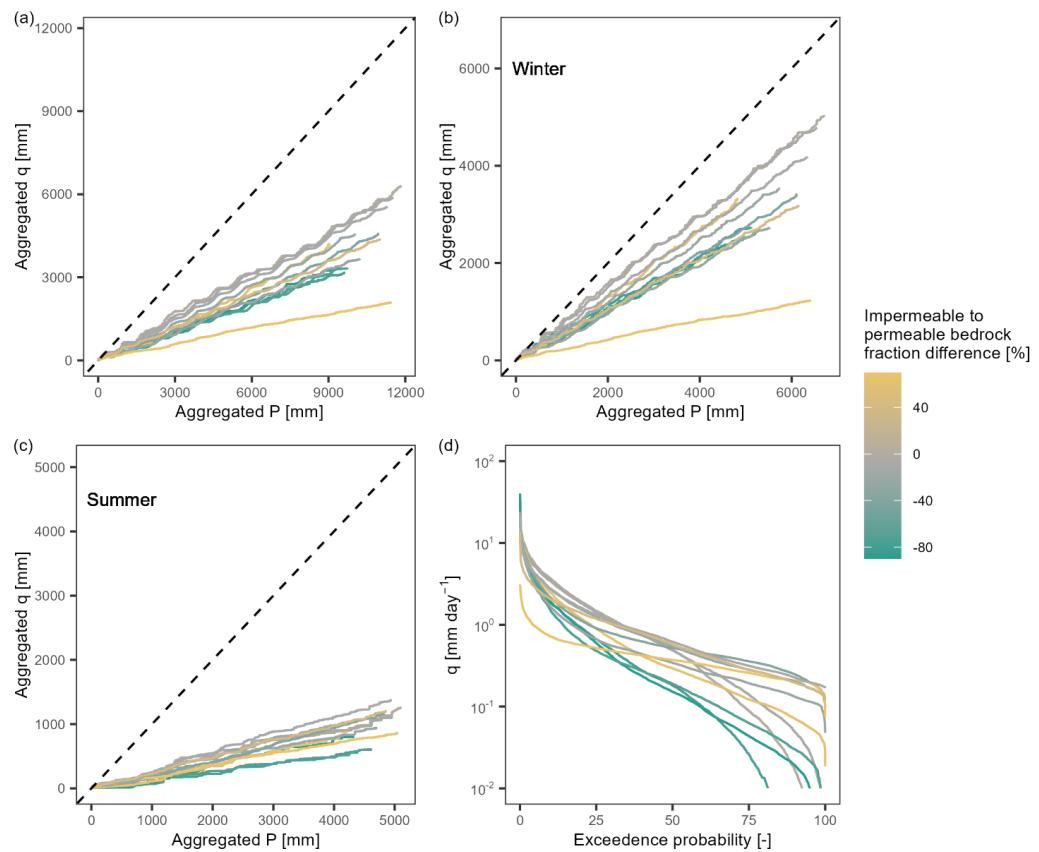
585

Figure A1: Streamflow generation in the 12 nested catchments: (a) double mass curves of aggregated precipitation versus streamflow, (b) double mass curves for winter values only, (c) double mass curves for summer values only, and (d) flow duration curves of specific streamflow. The dotted lines in plots (a), (b) and (c) represent 1:1 lines. The colour shading corresponds to the difference of the fraction of permeable bedrock (i.e. sandstone and conglomerates) minus the fraction of impermeable bedrock (i.e. marls and claystone).
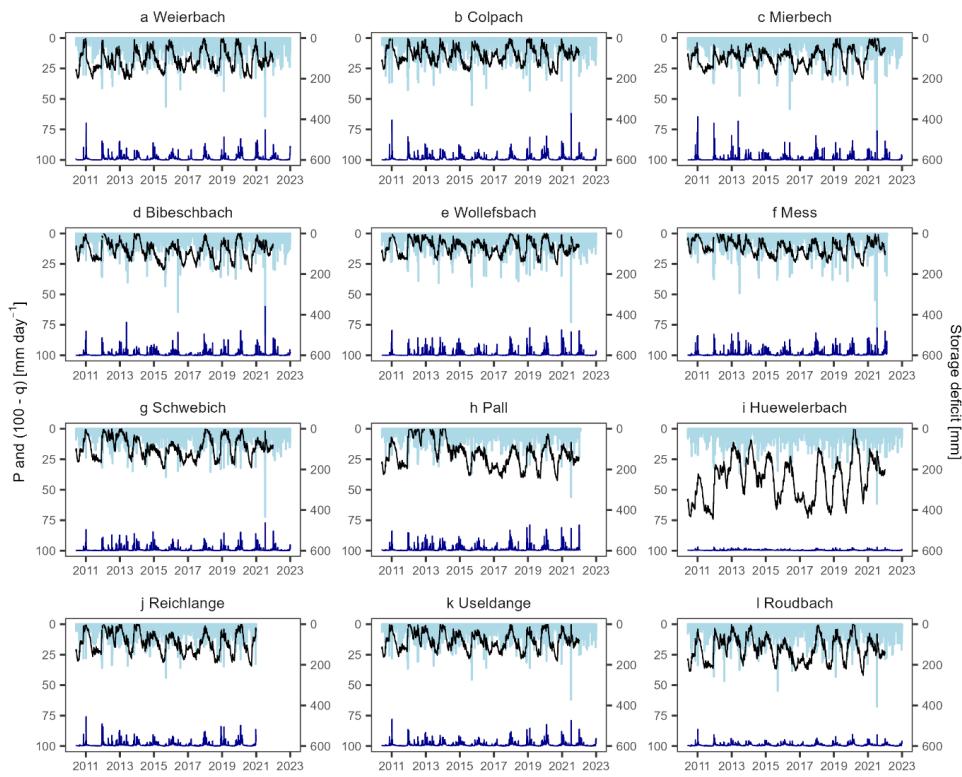
590

Figure A2: Daily precipitation (P, light blue bars), specific streamflow (q, dark blue line), and storage deficit (D, black line), in the 12 nested catchments of the Alzette basin.
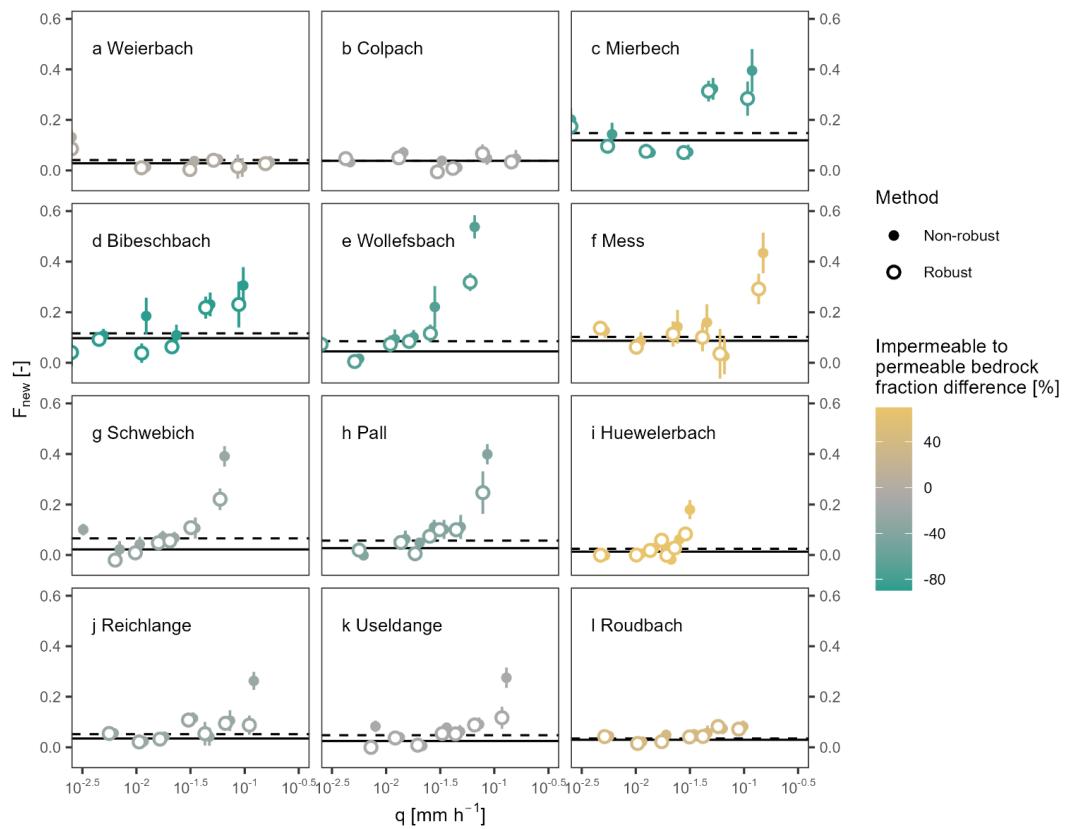
595

Appendix B

Figure B1: Profiles of the fractions of water younger than ~ 16 days (F_{new}) for daily mean specific streamflow quantiles (0-20, 20-40,
40-60, 60-70, 80-90, 90-100), and respective standard errors, calculated using the robust (empty circles) and non-robust (full circles)
solving algorithm from Kirchner (2019). The solid lines represent the robust F_{new} obtained for each of the catchments; the dotted
lines were obtained with the non-robust method. The colour shading corresponds to the difference of the fraction of permeable
bedrock (i.e. sandstone and conglomerates) minus the fraction of impermeable bedrock (i.e. marls and claystone).
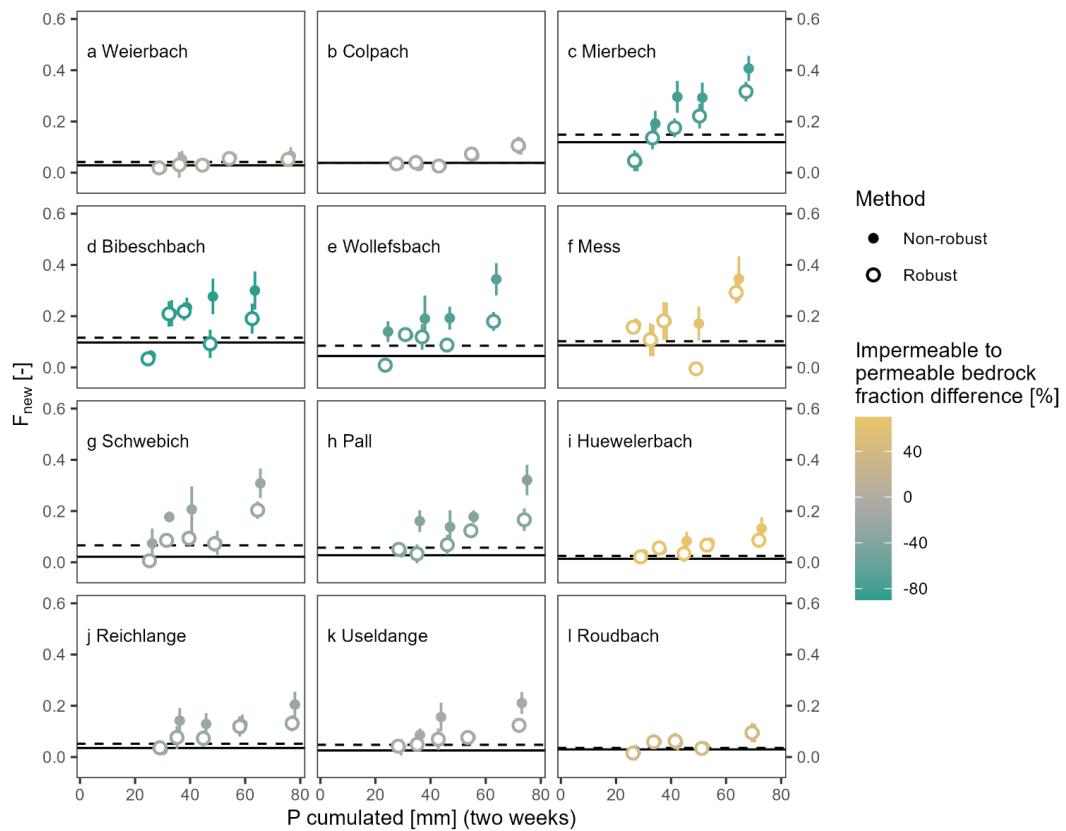
605

Figure B2: Profiles of the fractions water younger than ~ 16 days (F_{new}) for precipitation deciles >50% during the two weeks, and respective standard errors, calculated with the robust (empty circles) and non-robust (full circles) estimation method. The solid lines represent the robust F_{new} obtained for each of the twelve catchments; the dotted lines were obtained with the non-robust method. The colour shading corresponds to the difference of the fraction of permeable bedrock (i.e. sandstone and conglomerates) minus the
610 **fraction of impermeable bedrock (i.e. marls and claystone). The results imply higher F_{new} in catchments with impermeable bedrock geologies and an overall increase with increasing antecedent precipitation, which is more pronounced in catchments with a significant fraction of marls and claystone.**
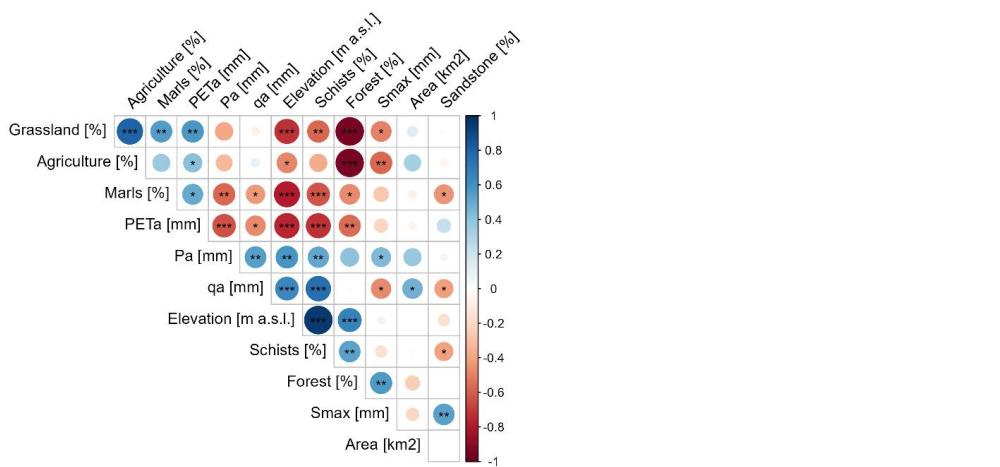
615 **Appendix C**

Figure C1: Correlation matrix (Pearson's r, colour scale) of the parameters defining the physiographic characteristics of the nested catchments extracted from the CAMELS-LUX database (Nijzink et al., 2024) using the corrplot package in R (Wei and Simko, 2021). Significance levels (0.001, 0.01, 0.05) are indicated by the stars (***, **, *). Results show that land use, bedrock geology, catchment elevation, and hydrometric values in our set of nested catchments are statistically correlated to some degree. Only the fraction of sandstones, the catchment area and the maximum storage capacity appear to be less correlated to other catchment characteristics.

Data availability

The data that support the findings of this study are available from the corresponding author upon reasonable request.

Author contribution

Competing interests

Some authors are members of the editorial board of journal Hydrology and Earth System Sciences.

Acknowledgements

References

640 Allen, M. R. and Ingram, W. J.: Constraints on future changes in climate and the hydrologic cycle, Nature, 419, 224–232, https://doi.org/10.1038/nature01092, 2002.

Allen, S. T., von Freyberg, J., Weiler, M., Goldsmith, G. R., and Kirchner, J. W.: The Seasonal Origins of Streamwater in Switzerland, Geophys. Res. Lett., 46, 10425–10434, https://doi.org/10.1029/2019GL084552, 2019.

Angermann, L., Jackisch, C., Allroggen, N., Sprenger, M., Zehe, E., Tronicke, J., Weiler, M., and Blume, T.: Form and function 645 in hillslope hydrology: Characterization of subsurface flow based on response observations, Hydrol. Earth Syst. Sci., 21, 3727–3748, https://doi.org/10.5194/hess-21-3727-2017, 2017.

APC - Administration des ponts et chaussées: Carte géologique harmonisée, https://geocatalogue.geoportail.lu/geonetwork/srv/fre/catalog.search#/metadata/542a0caa-4b33-4019-8ce7-b8541b436106, accessed: 2024-12-10, 2022.

650 Asano, Y., Suzuki, S. N., and Kawasaki, M.: Peak discharges per unit area increase with catchment area in a high-relief mountains with permeable sedimentary bedrock, J. Hydrol., 610, 127876, https://doi.org/10.1016/j.jhydrol.2022.127876, 2022.

Atwood, A., Hille, M., Clark, M. K., Rengers, F., Ntarlagiannis, D., Townsend, K., and West, A. J.: Importance of subsurface water for hydrological response during storms in a post-wildfire bedrock landscape, Nat. Commun., 14, 655 https://doi.org/10.1038/s41467-023-39095-z, 2023.

Benettin, P., Rinaldo, A., and Botter, G.: Tracking residence times in hydrological systems: forward and backward formulations, 5213, 5203–5213, https://doi.org/10.1002/hyp.10513, 2015.

Benettin, P., Rodriguez, N. B., Sprenger, M., Kim, M., Klaus, J., Harman, C. J., van der Velde, Y., Hrachowitz, M., Botter, G., McGuire, K. J., Kirchner, J. W., Rinaldo, A., and McDonnell, J. J.: Transit Time Estimation in Catchments: Recent 660 Developments and Future Directions, Water Resour. Res., 58, 1–36, https://doi.org/10.1029/2022WR033096, 2022.

Berghuijs, W. R., Woods, R. A., Hutton, C. J., and Sivapalan, M.: Dominant flood generating mechanisms across the United States, Geophys. Res. Lett., 43, 4382–4390, https://doi.org/10.1002/2016GL068070, 2016.

Blöschl, G., Bárdossy, A., Koutsoyiannis, D., Kundzewicz, Z. W., Littlewood, I., Montanari, A., and Savenije, H.: On the future of journal publications in hydrology, Water Resour. Res., 50, 2795–2797, https://doi.org/10.1002/2014WR015613, 665 2014.

Blöschl, G., Hall, J., Parajka, J., Perdigão, R. A. P., Merz, B., Arheimer, B., Aronica, G. T., Bilibashi, A., Bonacci, O., Borga, M., Čanjevac, I., Castellarin, A., Chirico, G. B., Claps, P., Fiala, K., Frolova, N., Gorbachova, L., Gül, A., Hannaford, J., Harrigan, S., Kireeva, M., Kiss, A., Kjeldsen, T. R., Kohnová, S., Koskela, J. J., Ledvinka, O., Macdonald, N., Mavrova-Guirguinova, M., Mediero, L., Merz, R., Molnar, P., Montanari, A., Murphy, C., Osuch, M., Ovcharuk, V., Radevski, I., 670 Rogger, M., Salinas, J. L., Sauquet, E., Šraj, M., Szolgay, J., Viglione, A., Volpi, E., Wilson, D., Zaimi, K., and Živković, N.: Changing climate shifts timing of European floods, Science (80-.)., 357, 588–590, https://doi.org/10.1126/science.aan2506, 2017.

Botter, G., Bertuzzo, E., and Rinaldo, A.: Catchment residence and travel time distributions: The master equation, Geophys. Res. Lett., 38, 1–6, https://doi.org/10.1029/2011GL047666, 2011.

675   BRGM - Bureau de Recherches Géologiques et Minière: Téléchargement des cartes géologiques départementales à 1/50 000 (Bd Charm-50), https://infoterre.brgm.fr/formulaire/telechargement-cartes-geologiques-departementales-150-000-bd-charm-50, accessed: 2024-12-10, 2020.

Burt, E. I., Goldsmith, G. R., Cruz-De Hoyos, R. M., Ccahuana Quispe, A. J., and West, A. J.: The seasonal origins and ages of water provisioning streams and trees in a tropical montane cloud forest, Hydrol. Earth Syst. Sci., 27, 4173–4186,

680   https://doi.org/10.5194/hess-27-4173-2023, 2023.

Creutzfeldt, B., Troch, P. A., Güntner, A., Ferré, T. P. A., Graeff, T., and Merz, B.: Storage-discharge relationships at different catchment scales based on local high-precision gravimetry, Hydrol. Process., 28, 1465–1475, https://doi.org/10.1002/hyp.9689, 2014.

Dansgaard, W.: Stable isotopes in precipitation, Tellus, 16, 436–468, https://doi.org/10.3402/tellusa.v16i4.8993, 1964.

685   DeWalle, D. R., Edwards, P. J., Swistock, B. R., Aravena, R., and Drimmie, R. J.: Seasonal isotope hydrology of three appalachian forest catchments, Hydrol. Process., 11, 1895–1906, https://doi.org/10.1002/(sici)1099-1085(199712)11:15<1895::aid-hyp538>3.0.co;2-#, 1997.

Douinot, A., Iffly, J. F., Tailliez, C., Meisch, C., and Pfister, L.: Flood patterns in a catchment with mixed bedrock geology and a hilly landscape: identification of flashy runoff contributions during storm events, Hydrol. Earth Syst. Sci., 26, 5185–

690   5206, https://doi.org/10.5194/hess-26-5185-2022, 2022.

Ehret, U., Gupta, H. V., Sivapalan, M., Weijs, S. V., Schymanski, S. J., Blöschl, G., Gelfan, A. N., Harman, C., Kleidon, A., Bogaard, T. A., Wang, D., Wagener, T., Scherer, U., Zehe, E., Bierkens, M. F. P., Di Baldassarre, G., Parajka, J., Van Beek, L. P. H., Van Griensven, A., Westhoff, M. C., and Winsemius, H. C.: Advancing catchment hydrology to deal with predictions under change, Hydrol. Earth Syst. Sci., 18, 649–671, https://doi.org/10.5194/hess-18-649-2014, 2014.

695   Fan, Y., Clark, M., Lawrence, D. M., Swenson, S., Band, L. E., Brantley, S. L., Brooks, P. D., Dietrich, W. E., Flores, A., Grant, G., Kirchner, J. W., Mackay, D. S., McDonnell, J. J., Milly, P. C. D., Sullivan, P. L., Tague, C., Ajami, H., Chaney, N., Hartmann, A., Hazenberg, P., McNamara, J., Pelletier, J., Perket, J., Rouholahnejad-freund, E., Wagener, T., Zeng, X., Beighley, E., Buzan, J., Huang, M., Livneh, B., Mohanty, B. P., Nijssen, B., Safeeq, M., Shen, C., Verseveld, W., Volk, J., and Yamazaki, D.: Hillslope Hydrology in Global Change Research and Earth System Modeling, Water Resour. Res., 55,

700   1737–1772, https://doi.org/10.1029/2018WR023903, 2019.

Feng, X., Faiia, A. M., and Posmentier, E. S.: Seasonality of isotopes in precipitation: A global perspective, J. Geophys. Res. Atmos., 114, 1–13, https://doi.org/10.1029/2008JD011279, 2009.

Fenicia, F., Kavetski, D., Savenije, H. H. G., Clark, M. P., Schoups, G., Pfister, L., and Freer, J.: Catchment properties, function, and conceptual model representation: Is there a correspondence?, Hydrol. Process., 28, 2451–2467,

705   https://doi.org/10.1002/hyp.9726, 2014.

Floriancic, M. G., Stockinger, M. P., Kirchner, J. W., and Stumpp, C.: New water fractions and their relationships to climate and catchment properties across Alpine rivers, EGUsphere, 2023, 1–32, 2023.

Floriancic, M. G., Allen, S. T., and Kirchner, J. W.: Young and new water fractions in soil and hillslope waters, Hydrol. Earth Syst. Sci., 28, 4295–4308, https://doi.org/10.5194/hess-28-4295-2024, 2024.

710   Von Freyberg, J., Allen, S. T., Seeger, S., Weiler, M., and Kirchner, J. W.: Sensitivity of young water fractions to hydro-climatic forcing and landscape properties across 22 Swiss catchments, Hydrol. Earth Syst. Sci., 22, 3841–3861, https://doi.org/10.5194/hess-22-3841-2018, 2018.

Gentile, A., Canone, D., Ceperley, N., Gisolo, D., Previati, M., Zuecco, G., Schaefli, B., and Ferraris, S.: Towards a conceptualization of the hydrological processes behind changes of young water fraction with elevation: A focus on

715   mountainous alpine catchments, Hydrol. Earth Syst. Sci., 27, 2301–2323, https://doi.org/10.5194/hess-27-2301-2023, 2023.

Glaser, B., Klaus, J., Frei, S., Frentress, J., Pfister, L., and Hopp, L.: On the value of surface saturated area dynamics mapped with thermal infrared imagery for modeling the hillslope-riparian-stream continuum, Water Resour. Res., 52, 8317–8342, https://doi.org/10.1002/2015WR018414, 2016.

Glaser, B., Jackisch, C., Hopp, L., and Klaus, J.: How Meaningful are Plot-Scale Observations and Simulations of Preferential
720 Flow for Catchment Models?, Vadose Zo. J., 18, 1–18, https://doi.org/10.2136/vzj2018.08.0146, 2019.

Glaser, B., Antonelli, M., Hopp, L., and Klaus, J.: Intra-catchment variability of surface saturation - Insights from physically based simulations in comparison with biweekly thermal infrared image observations, Hydrol. Earth Syst. Sci., 24, 1393–1413, https://doi.org/10.5194/hess-24-1393-2020, 2020.

Gourdol, L., Stewart, M. K., Morgenstern, U., and Pfister, L.: Short high-accuracy tritium data time series for assessing
725 groundwater mean transit times in the vadose and saturated zones of the Luxembourg Sandstone aquifer, Hydrol. Earth Syst. Sci., 28, 3519–3547, https://doi.org/10.5194/hess-28-3519-2024, 2024.

Gräler B., Pebesma E., Heuvelink G. "Spatio-Temporal Interpolation using gstat." The R Journal, 8, 204-218. https://journal.r-project.org/archive/2016/RJ-2016-014/index.html, 2016.

Harman, C. J.: Time-variable transit time distributions and transport: Theory and application to storage-dependent transport of
730 chloride in a watershed, Water Resour. Res., 51, 1–30, https://doi.org/10.1002/2014WR015707, 2015.

Hellebrand, H., Hoffmann, L., Juilleret, J., and Pfister, L.: Assessing winter storm flow generation by means of permeability of the lithology and dominating runoff production processes, Hydrol. Earth Syst. Sci., 11, 1673–1682, https://doi.org/10.5194/hess-11-1673-2007, 2007.

Hissler, C., Martínez-Carreras, N., Barnich, F., Gourdol, L., Iffly, J. F., Juilleret, J., Klaus, J., and Pfister, L.: The Weierbach
735 experimental catchment in Luxembourg: A decade of critical zone monitoring in a temperate forest - from hydrological investigations to ecohydrological perspectives, Hydrol. Process., 35, 1–7, https://doi.org/10.1002/hyp.14140, 2021.

Hrachowitz, M., Soulsby, C., Tetzlaff, D., and Speed, M.: Catchment transit times and landscape controls—does scale matter?, Hydrol. Process., 24, 117–125, https://doi.org/10.1002/hyp.7510, 2010.

Hrachowitz, M., Savenije, H. H. G., Blöschl, G., McDonnell, J. J., Sivapalan, M., Pomeroy, J. W., Arheimer, B., Blume, T.,
740 Clark, M. P., Ehret, U., Fenicia, F., Freer, J. E., Gelfan, A., Gupta, H. V., Hughes, D. A., Hut, R. W., Montanari, A., Pande, S., Tetzlaff, D., Troch, P. A., Uhlenbrook, S., Wagener, T., Winsemius, H. C., Woods, R. A., Zehe, E., and Cudennec, C.: A decade of Predictions in Ungauged Basins (PUB)-a review, Hydrol. Sci. J., 58, 1198–1255, https://doi.org/10.1080/02626667.2013.803183, 2013.

IAEA: Reference Sheet for International Measurement Standards VSMOW2, SLAP2, Int. At. Energy Agency, 8, 2017.

745 Kaplan, N. H., Blume, T., and Weiler, M.: Event controls on intermittent streamflow in a temperate climate, Hydrol. Earth Syst. Sci., 26, 2671–2696, https://doi.org/10.5194/hess-26-2671-2022, 2022.

Katsuyama, M., Ohte, N., and Kabeya, N.: Effects of bedrock permeability on hillslope and riparian groundwater dynamics in a weathered granite catchment, Water Resour. Res., 41, 1–11, https://doi.org/10.1029/2004WR003275, 2005.

Kirchner, J. W.: Getting the right answers for the right reasons: Linking measurements, analyses, and models to advance the
750 science of hydrology, Water Resour. Res., 42, 1–5, https://doi.org/10.1029/2005WR004362, 2006.

Kirchner, J. W.: Aggregation in environmental systems-Part 1: Seasonal tracer cycles quantify young water fractions, but not mean transit times, in spatially heterogeneous catchments, Hydrol. Earth Syst. Sci., 20, 279–297, https://doi.org/10.5194/hess-20-279-2016, 2016a.

Kirchner, J. W.: Aggregation in environmental systems-Part 2: Catchment mean transit times and young water fractions under
755 hydrologic nonstationarity, Hydrol. Earth Syst. Sci., 20, 299–328, https://doi.org/10.5194/hess-20-299-2016, 2016b.

Kirchner, J. W.: Quantifying new water fractions and transit time distributions using ensemble hydrograph separation : theory and benchmark tests, Hydrol. Earth Syst. Sci., 23, 303–349, 2019.

Kirchner, J. W. and Knapp, J. L. A.: Technical note : Calculation scripts for ensemble hydrograph separation, Hydrol. Earth Syst. Sci., 24, 5539–5558, 2020.

760 Kirchner, J. W.: Characterizing nonlinear, nonstationary, and heterogeneous hydrologic behavior using Ensemble Rainfall-Runoff Analysis (ERRA): proof of concept, Hydrol. Earth Syst. Sci. Discuss., 1–42, 2024.

Knapp, J. L. A., Neal, C., Schlumpf, A., Neal, M., and Kirchner, J. W.: New water fractions and transit time distributions at Plynlimon, Wales, estimated from stable water isotopes in precipitation and streamflow, 23, 4367–4388, 2019.

Loritz, R., Hassler, S. K., Jackisch, C., Allroggen, N., Van Schaik, L., Wienhöfer, J., and Zehe, E.: Picturing and modeling
765 catchments by representative hillslopes, Hydrol. Earth Syst. Sci., 21, 1225–1249, https://doi.org/10.5194/hess-21-1225-2017, 2017.

Lutz, S. R., Krieg, R., Müller, C., Zink, M., Knöller, K., Samaniego, L., and Merz, R.: Spatial Patterns of Water Age: Using Young Water Fractions to Improve the Characterization of Transit Times in Contrasting Catchments, Water Resour. Res., 54, 4767–4784, https://doi.org/10.1029/2017WR022216, 2018.

770 Maneta, M. P., Soulsby, C., Kuppel, S., and Tetzlaff, D.: Conceptualizing catchment storage dynamics and nonlinearities, Hydrol. Process., 32, 3299–3303, https://doi.org/10.1002/hyp.13262, 2018.

Martínez-Carreras, N., Hissler, C., Gourdol, L., Klaus, J., Juilleret, J., Iffly, J. F., and Pfister, L.: Storage controls on the generation of double peak hydrographs in a forested headwater catchment, J. Hydrol., 543, 255–269, https://doi.org/10.1016/j.jhydrol.2016.10.004, 2016.

775 Masaoka, N., Kosugi, K., and Fujimoto, M.: Bedrock Groundwater Catchment Area Unveils Rainfall-Runoff Processes in Headwater Basins, Water Resour. Res., 57, 1–18, https://doi.org/10.1029/2021WR029888, 2021.

McDonnell, J. J., Sivapalan, M., Vaché, K., Dunn, S., Grant, G., Haggerty, R., Hinz, C., Hooper, R., Kirchner, J., Roderick, M. L., Selker, J., and Weiler, M.: Moving beyond heterogeneity and process complexity: A new vision for watershed hydrology, Water Resour. Res., 43, 1–6, https://doi.org/10.1029/2006WR005467, 2007.Nijzink, J., Loritz, R., Gourdol, L.,
780 Iffly, J. F., Zoccatelli, D. and Pfister, L.: CAMELS-LUX: Highly resolved hydro-meteorological and atmospheric data for physiographically characterized catchments around Luxembourg, Earth Syst. Sci. Data, essd-2024-482, 2024 [submitted 20 Oct 2024].

Pebesma E.J. (2004). "Multivariable geostatistics in S: the gstat package." Computers & Geosciences, 30, 683-691.

Pfister, L. and Kirchner, J. W.: Debates—Hypothesis testing in hydrology: Theory and practice, Water Resour. Res., 53, 1792–
785 1798, https://doi.org/10.1002/2016WR020116, 2017.

Pfister, L., Drogue, G., El Idrissi, A., Iffly, J. F., Poirier, C., and Hoffmann, L.: Spatial variability of trends in the rainfall-runoff relationship: A mesoscale study in the Mosel basin, Clim. Change, 66, 67–87, https://doi.org/10.1023/B:CLIM.0000043160.26398.4c, 2004.

Pfister, L., Martínez-Carreras, N., Hissler, C., Klaus, J., Carrer, G. E., Stewart, M. K., and McDonnell, J. J.: Bedrock geology
790 controls on catchment storage, mixing, and release: A comparative analysis of 16 nested catchments, Hydrol. Process., 31, 1828–1845, https://doi.org/10.1002/hyp.11134, 2017.

Pfister, L., Hissler, C., Iffly, J. F., Coenders, M., Teuling, R., Arens, A., and Cammeraat, L. H.: Contrasting Hydrologic Response in the Cuesta Landscapes of Luxembourg, in: The Luxembourg Gutland Landscape, Springer International Publishing, Cham, 73–87, https://doi.org/10.1007/978-3-319-65543-7_4, 2018.

795 Pfister, L., Bonanno, E., Fabiani, G., Gourdol, L., Hissler, C., Huck, V., Iffly, J. F., Keim, R., Martínez-Carreras, N., Mestdagh, X., Montemagno, A., Penna, D., Schymanski, S., and Zehe, E.: Fast motion view of a headwater creek—A hydrological year seen through time-lapse photography, Hydrol. Process., 37, 1–10, https://doi.org/10.1002/hyp.15026, 2023.

Pinder, G. F. and Jones, J. F.: Determination of the ground-water component of peak discharge from the chemistry of total runoff, Water Resour. Res., 5, 438–445, https://doi.org/10.1029/WR005i002p00438, 1969.

800   Remondi, F., Kirchner, J. W., Burlando, P., and S., F.: Water Flux Tracking With a Distributed Hydrological Model to Quantify
      Controls on the Spatio - temporal Variability of Transit Time Distributions Water Resources Research, Water Resour. Res.,
      54, 3081–3099, https://doi.org/10.1002/2017WR021689, 2018.

      Rinaldo, A., Benettin, P., Harman, C. J., Hrachowitz, M., McGuire, K. J., van der Velde, Y., Bertuzzo, E., and Botter, G.:
      Storage selection functions: A coherent framework for quantifying how catchments store and release water and solutes, Water

805   Resour. Res., 51, 4840–4847, https://doi.org/10.1002/2015WR017273, 2015.

      Rodriguez, N. B., McGuire, K. J., and Klaus, J.: Time-Varying Storage–Water Age Relationships in a Catchment With a
      Mediterranean Climate, Water Resour. Res., 54, 3988–4008, https://doi.org/10.1029/2017WR021964, 2018.

      Sayama, T., Mcdonnell, J. J., Dhakal, A., and Sullivan, K.: How much water can a watershed store?, Hydrol. Process., 25,
      3899–3908, https://doi.org/10.1002/hyp.8288, 2011.

810   Scaini, A., Audebert, M., Hissler, C., Fenicia, F., Gourdol, L., Pfister, L., and Beven, K. J.: Velocity and celerity dynamics at
      plot scale inferred from artificial tracing experiments and time-lapse ERT, J. Hydrol., 546, 28–43,
      https://doi.org/10.1016/j.jhydrol.2016.12.035, 2017.

      Scaini, A., Hissler, C., Fenicia, F., Juilleret, J., Iffly, J. F., Pfister, L., and Beven, K.: Hillslope response to sprinkling and
      natural rainfall using velocity and celerity estimates in a slate-bedrock catchment, J. Hydrol., 558, 366–379,

815   https://doi.org/10.1016/j.jhydrol.2017.12.011, 2018.

      Schaefli, B., Harman, C. J., Sivapalan, M., and Schymanski, S. J.: HESS Opinions: Hydrologic predictions in a changing
      environment: Behavioral modeling, Hydrol. Earth Syst. Sci., 15, 635–646, https://doi.org/10.5194/hess-15-635-2011, 2011.

      Seibert, J. and McDonnell, J. J.: Gauging the Ungauged Basin: Relative Value of Soft and Hard Data, J. Hydrol. Eng., 20, 1–
      6, https://doi.org/10.1061/(asce)he.1943-5584.0000861, 2015.

820   Slater, L. J. and Wilby, R. L.: Measuring the changing pulse of rivers, Science (80-.)., 357, 552,
      https://doi.org/10.1126/science.aao2441, 2017.

      Soulsby, C., Tetzlaff, D., and Hrachowitz, M.: Tracers and transit times: windows for viewing catchment scale storage?,
      Hydrol. Process., 23, 3503–3507, https://doi.org/10.1002/hyp.7501, 2009.

      Thornthwaite, C.W. (1948). An approach toward a rational classification of climate. Geographical Review, 38, 55–94.

825   Troch, P. A., Lahmers, T., Meira, A., Mukherjee, R., Pedersen, J. W., Roy, T., and Valdés-Pineda, R.: Catchment coevolution:
      A useful framework for improving predictions of hydrological change?, Water Resour. Res., 51, 4903–4922,
      https://doi.org/10.1002/2015WR017032, 2015.

      Tromp-Van Meerveld, H. J. and McDonnell, J. J.: Threshold relations in subsurface stormflow: 2. The fill and spill hypothesis,
      Water Resour. Res., 42, 1–11, https://doi.org/10.1029/2004WR003800, 2006.

830   Uchida, T., McDonnell, J. J., and Asano, Y.: Functional intercomparison of hillslopes and small catchments by examining
      water source, flowpath and mean residence time, J. Hydrol., 327, 627–642, https://doi.org/10.1016/j.jhydrol.2006.02.037,
      2006.

      Weedon, G. P., Robinson, E. L., Bloomfield, J. P., Turner, S., Crane, E. J., and Best, M. J.: Geological controls of discharge
      variability in the Thames Basin, UK from cross-spectral analyses: Observations versus modelling, J. Hydrol., 625, 130104,

835   https://doi.org/10.1016/j.jhydrol.2023.130104, 2023.

      Wrede, S., Fenicia, F., Martínez-carreras, N., Juilleret, J., Hissler, C., Krein, A., Savenije, H. H. G., Uhlenbrook, S., Kavetski,
      D., and Laurent, P.: Towards more systematic perceptual model development : a case study using 3 Luxembourgish
      catchments, 2750, 2731–2750, https://doi.org/10.1002/hyp.10393, 2015.

      Wei, T. and Simko, V., R package 'corrplot': Visualization of a Correlation Matrix   (Version 0.92), Available from

840   https://github.com/taiyun/corrplot, 2021.

      Zehe, E., Ehret, U., Pfister, L., Blume, T., Schröder, B., Westhoff, M., Jackisch, C., Schymanski, S. J., Weiler, M., Schulz, K.,
      Allroggen, N., Tronicke, J., Van Schaik, L., Dietrich, P., Scherer, U., Eccard, J., Wulfmeyer, V., and Kleidon, A.: HESS

Opinions: From response units to functional units: A thermodynamic reinterpretation of the HRU concept to link spatial organization and functioning of intermediate scale catchments, Hydrol. Earth Syst. Sci., 18, 4635–4655, https://doi.org/10.5194/hess-18-4635-2014, 2014.